



Article

Mg₁₂O₁₂ and Be₁₂O₁₂ Nanocages as Sorbents and Sensors for H₂S and SO₂ Gases: A Theoretical Approach

H. M. Badran ¹, Kh. M. Eid ^{2,3}, Sotirios Baskoutas ⁴ and H. Y. Ammar ^{1,*}

¹ Physics Department, College of Science and Arts, Najran University, Najran 11001, Saudi Arabia; hmbadran@nu.edu.sa

² Physics Department, Faculty of Education, Ain Shams University, Cairo 11566, Egypt; khmeid@yahoo.com

³ Department of Physics, College of Science and Arts, Qassim University, Albukayriyah 52725, Saudi Arabia

⁴ Department of Materials Science, University of Patras, 26504 Patras, Greece; bask@upatras.gr

* Correspondence: hyammar@hotmail.com

Abstract: Theoretical calculations based on the Density Functional Theory (DFT) have been performed to investigate the interaction of H₂S as well SO₂ gaseous molecules at the surfaces of Be₁₂O₁₂ and Mg₁₂O₁₂ nano-cages. The results show that a Mg₁₂O₁₂ nano-cage is a better sorbent than a Be₁₂O₁₂ nano-cage for the considered gases. Moreover, the ability of SO₂ gas to be adsorbed is higher than that of H₂S gas. The HOMO–LUMO gap (E_g) of Be₁₂O₁₂ nano-cage is more sensitive to SO₂ than H₂S adsorption, while the E_g value of Mg₁₂O₁₂ nano-cage reveals higher sensitivity to H₂S than SO₂ adsorption. The molecular dynamic calculations show that the H₂S molecule cannot be retained at the surface of a Be₁₂O₁₂ nano-cage within 300–700 K and cannot be retained on a Mg₁₂O₁₂ nano-cage at 700 K, while the SO₂ molecule can be retained at the surfaces of Be₁₂O₁₂ and Mg₁₂O₁₂ nano-cages up to 700 K. Moreover, the thermodynamic calculations indicate that the reactions between H₂S as well SO₂ with Be₁₂O₁₂ and Mg₁₂O₁₂ nano-cages are exothermic. Our results suggest that we can use Be₁₂O₁₂ and Mg₁₂O₁₂ nano-cages as sorbents as well as sensors for H₂S and SO₂ gases.

Keywords: adsorption of H₂S and SO₂; BeO and MgO nano-cages; density functional theory; thermodynamics; molecular dynamics



Citation: Badran, H.M.; Eid, K.M.; Baskoutas, S.; Ammar, H.Y. Mg₁₂O₁₂ and Be₁₂O₁₂ Nanocages as Sorbents and Sensors for H₂S and SO₂ Gases: A Theoretical Approach. *Nanomaterials* **2022**, *12*, 1757. <https://doi.org/10.3390/nano12101757>

Academic Editor: J. Karl Johnson

Received: 22 April 2022

Accepted: 19 May 2022

Published: 21 May 2022

Publisher's Note: MDPI stays neutral with regard to jurisdictional claims in published maps and institutional affiliations.



Copyright: © 2022 by the authors. Licensee MDPI, Basel, Switzerland. This article is an open access article distributed under the terms and conditions of the Creative Commons Attribution (CC BY) license (<https://creativecommons.org/licenses/by/4.0/>).

1. Introduction

Recently, great efforts have been made to develop novel gas sensors and detectors as well as gas-removing materials. This is to control the pollutant gases broadly produced from industrial activities and burning fuel, etc. The toxic H₂S and SO₂ gases are produced as byproducts from SF₆ decomposition, which is widely used as an insulating gas in high-voltage transformers and circuit breakers [1–4]. H₂S is mostly found in crude petroleum, natural gas, and coal gasification. In addition, some organic materials decompose, releasing H₂S [5–7]. H₂S is also released in many industries such as the paper industry and biomass fermenters [7,8]. The combustion of sulfur-containing fossil fuels releases SO₂ into the air, and SO₂ is naturally released as a byproduct of volcanic activity [9,10]. The H₂S as well SO₂ gases pose several hazards to the environment and human health. H₂S exposure leads to coughing, eye irritation, and a runny nose, harms the nervous system by killing the neurons and may cause death [11,12]. Moreover, H₂S is a corrosive gas and has devastating impacts on industrial catalysts [7,8]. SO₂ interacts with the air resulting in acidic rain which causes the corrosion of metals and disintegration of buildings [9,10]. Furthermore, SO₂ causes skin burning, eye irritation and respiratory system inflammation, and may cause death [7,13–15]. Therefore, several attempts have been made to utilize many materials as sorbents and detectors for H₂S and SO₂ gases, such as fullerene-like gallium nitride [16], CuO(111) surface [17], pristine graphene and graphene oxide [18], NH-decorated graphene [8], activated carbon, [19,20], pillared clays [21], zeolites [22], p-CuO/n-ZnO Heterojunction [23], Cu (100) and Au (100) surfaces [24,25], Cu

doped MoSe₂ [12], monolayer Janus MoSSe [26], aza-macrocycle [27], Cu-modified and Cu-embedded WSe₂ monolayers [28], porous N₄O₄-donor macrocyclic Schiff base [29] and MgO (100) surfaces [10].

Metal oxides have a significant consideration due to their several applications. They are usually utilized as substrates for epitaxial growth of multilayers and clusters, catalytic processes, hydrogen storage materials, sensors and sorbent materials [10,30–34]. Recently, nano-structures have been frequently utilized as gas detectors and sorbents due to their appropriate features such as their tiny size, precision, and reactivity [35–37].

Furthermore, Shamlouei et al. reported that nanocages with a X₁₂Y₁₂ structure are the most stable among (XY)_n nano-cages [38]. Ren et al. [39] have investigated (BeO)_N clusters and found that Be₁₂O₁₂ is one of the most feasible nano-cages. Ziemann and Castleman [40] have proven that a Mg₁₂O₁₂ nano-cage displays unique stability among (MgO)_n, n ≤ 90 nano-structures. The Mg–O bond in Mg₁₂O₁₂ nano-cages has an ionic character [38], while the Be–O bond has ionic and covalent characters [41], therefore one can expect different applications for Be₁₂O₁₂ and Mg₁₂O₁₂ nano-cages. Be₁₂O₁₂ and Mg₁₂O₁₂ have several applications; for instance, Be₁₂O₁₂ has been utilized as a catalyst to convert CH₄ into CH₃OH [42], an electro-conductive sensor for sulfur mustard [43], and a detector and sorbent for Mercaptopyridine [44], and Be₁₂O₁₂ and Mg₁₂O₁₂ have been utilized for hydrogen storage applications [45,46], detection and adsorption of Tabun [47]

According to our knowledge, the interaction of H₂S and SO₂ gases at the surfaces of Be₁₂O₁₂ and Mg₁₂O₁₂ nano-cages has not been investigated yet. Hence, the present work aims to shed light on the characteristics of the interaction of H₂S and SO₂ with Be₁₂O₁₂ and Mg₁₂O₁₂ nano-cages for adsorption and sensing applications using DFT calculations.

2. Methods

To investigate the adsorption characteristics of H₂S and SO₂ molecules onto Be₁₂O₁₂ and Mg₁₂O₁₂ nano-cages, DFT and DFT-D3 methods [48] are used at the B3LYP/6-31G(d,p) level. D3 is a version of Grimme’s dispersion [49]. B3 is Becke’s three-parameter exchange functional [50] and LYP is the correlation functional of Lee, Yang and Parr [51,52]. A geometrical optimization without any restriction is performed for the free gaseous molecules, bare nano-cages and gas/nano-cage complexes. The ionization potential (IP) is calculated as [10,37]:

$$IP = E_{\text{nano-cage}^+} - E_{\text{nano-cage}} \quad (1)$$

where $E_{\text{nano-cage}^+}$ is the energy of the nano-cage with one electron lost at the same geometrical structure of the neutrally charged nano-cage. The chemical potential (μ), hardness (η) and electrophilicity (ω) are calculated as [53,54]:

$$\mu \approx -\frac{1}{2} (E_{\text{HOMO}} + E_{\text{LUMO}}) \quad (2)$$

$$\eta \approx \frac{1}{2} (E_{\text{LUMO}} - E_{\text{HOMO}}) \quad (3)$$

$$\omega \approx \frac{\mu^2}{2\eta} \quad (4)$$

Molecular dynamic simulations via the Atom Centered Density Matrix Propagation molecular dynamics model (ADMP) as implemented in Gaussian 09 package are achieved for the investigated nano-cages and gas/nano-cage complexes.

The adsorption energy (E_{ads}) and the corrected adsorption energy ($E_{\text{ads}}^{\text{corr}}$) with basis set superposition error (BSSE) have been estimated as [55]:

$$E_{\text{ads}} = E_{\text{gas/nano-cage}} - (E_{\text{gas}} + E_{\text{nano-cage}}) \quad (5)$$

$$E_{\text{ads}}^{\text{corr}} = E_{\text{ads}} + E_{\text{BSSE}} \quad (6)$$

where $E_{\text{gas/nano-cage}}$, E_{gas} , and $E_{\text{nano-cage}}$ are the energies of gas/nano-cage complexes, free gas molecules, and bare nano-cages, respectively. The charge density difference ($\Delta\rho$) for the complexes is computed as:

$$\Delta\rho = \rho_{\text{gas/nano-cage}} - (\rho_{\text{gas}} + \rho_{\text{nano-cage}}) \quad (7)$$

where $\rho_{\text{gas/nano-cage}}$, ρ_{gas} , and $\rho_{\text{nano-cage}}$ are the charge densities for gas/nano-cage complexes, free gas molecules, and bare nano-cages, respectively.

Thermodynamic calculations are performed via vibrational calculations to predict enthalpies as well free energies for the considered gases, nano-cages, and gas-cages complexes. Enthalpy difference (ΔH) and free energy difference (ΔG) for gas/nano-cage complexes are evaluated as [56]:

$$\Delta H = H_{\text{gas/nano-cage}} - (H_{\text{gas}} + H_{\text{nano-cage}}) \quad (8)$$

where $H_{\text{gas/nano-cage}}$, $H_{\text{nano-cage}}$, and H_{gas} are the enthalpies for gas/nano-cage complexes, bare nano-cages and free gas molecules, respectively.

$$\Delta G = G_{\text{gas/nano-cage}} - (G_{\text{gas}} + G_{\text{nano-cage}}) \quad (9)$$

where $G_{\text{gas/nano-cage}}$, $G_{\text{nano-cage}}$, and G_{gas} are the free energies for gas/nano-cage complexes, bare nano-cages, and free gas molecules, respectively.

All the calculations have been carried out by Gaussian 09 program package [57]. GaussSum3.0 program is used to visualize the densities of states (DOS) [58]. Atomic charges are calculated for the considered structures via full natural bond orbital (NBO) analyses by using NBO version 3.1 [59].

3. Results and Discussions

3.1. Structural and Electronic Properties of $\text{Be}_{12}\text{O}_{12}$ and $\text{Mg}_{12}\text{O}_{12}$

The optimized structures for the scrutinized adsorbed gases H_2S and SO_2 , as well the adsorbent nano-cages $\text{Be}_{12}\text{O}_{12}$ and $\text{Mg}_{12}\text{O}_{12}$, are shown in Figure 1.

For H_2S gas, the S-H bond length and the H-S-H angle are 1.35 Å and 92.52°, respectively, while for SO_2 gas, the S-O bond length and the O-S-O angle are 1.46 Å and 119.16°, respectively, in good agreement with previous studies [10,29]. $\text{Be}_{12}\text{O}_{12}$, as well $\text{Mg}_{12}\text{O}_{12}$ nano-cages are constructed of eight hexagonal and six tetragonal rings. It is noticed that all the metallic (Be and Mg) and O sites are identical. These nano-cages have two metal-oxygen bond types. They are denoted as d_1 and d_2 in Figure 1, where d_1 shares a hexagon ring and a tetragon ring while d_2 shares two hexagon rings. The d_1 values are 1.58 and 1.95 Å, whereas the d_2 values are 1.52 and 1.90 Å for $\text{Be}_{12}\text{O}_{12}$ and $\text{Mg}_{12}\text{O}_{12}$, respectively, match well with the previous studies [39,60–63]. Table 1 represents the electronic properties of $\text{Be}_{12}\text{O}_{12}$ and $\text{Mg}_{12}\text{O}_{12}$ nano-cages.

The HOMO–LUMO energy gap (E_g) values for $\text{Be}_{12}\text{O}_{12}$ and $\text{Mg}_{12}\text{O}_{12}$ are 7.829 and 4.839 eV while the ionization potential (IP) values are 10.273 and 7.983 eV, respectively, in good agreement with the previous studies [10,30,31,39,44,60–63]. The lower IP value for the $\text{Mg}_{12}\text{O}_{12}$ nano-cage suggests its higher ability to donate electrons than the $\text{Be}_{12}\text{O}_{12}$ nano-cage. The atomic charges for the investigated nano-cage are calculated via natural bond orbital (NBO) analysis. For $\text{Be}_{12}\text{O}_{12}$, the atomic charges for Be and O sites are 1.186 and -1.186 e, while for $\text{Mg}_{12}\text{O}_{12}$, the atomic charges for Mg and O sites are 1.442 and -1.442 e, respectively. In other words, the charge polarization for the Mg–O bond is greater than that for the Be–O bond; therefore, the $\text{Mg}_{12}\text{O}_{12}$ is expected to be more reactive than $\text{Be}_{12}\text{O}_{12}$. This matches the calculated E_g , IP, η , and ω values, where the higher chemical stability and consequently lower reactivity for a molecule are marked by wide E_g , large IP, η , and low ω values [64–67]. Figure 2 illustrates the molecular electrostatic potential (MESP) for H_2S , SO_2 , $\text{Be}_{12}\text{O}_{12}$, and $\text{Mg}_{12}\text{O}_{12}$.

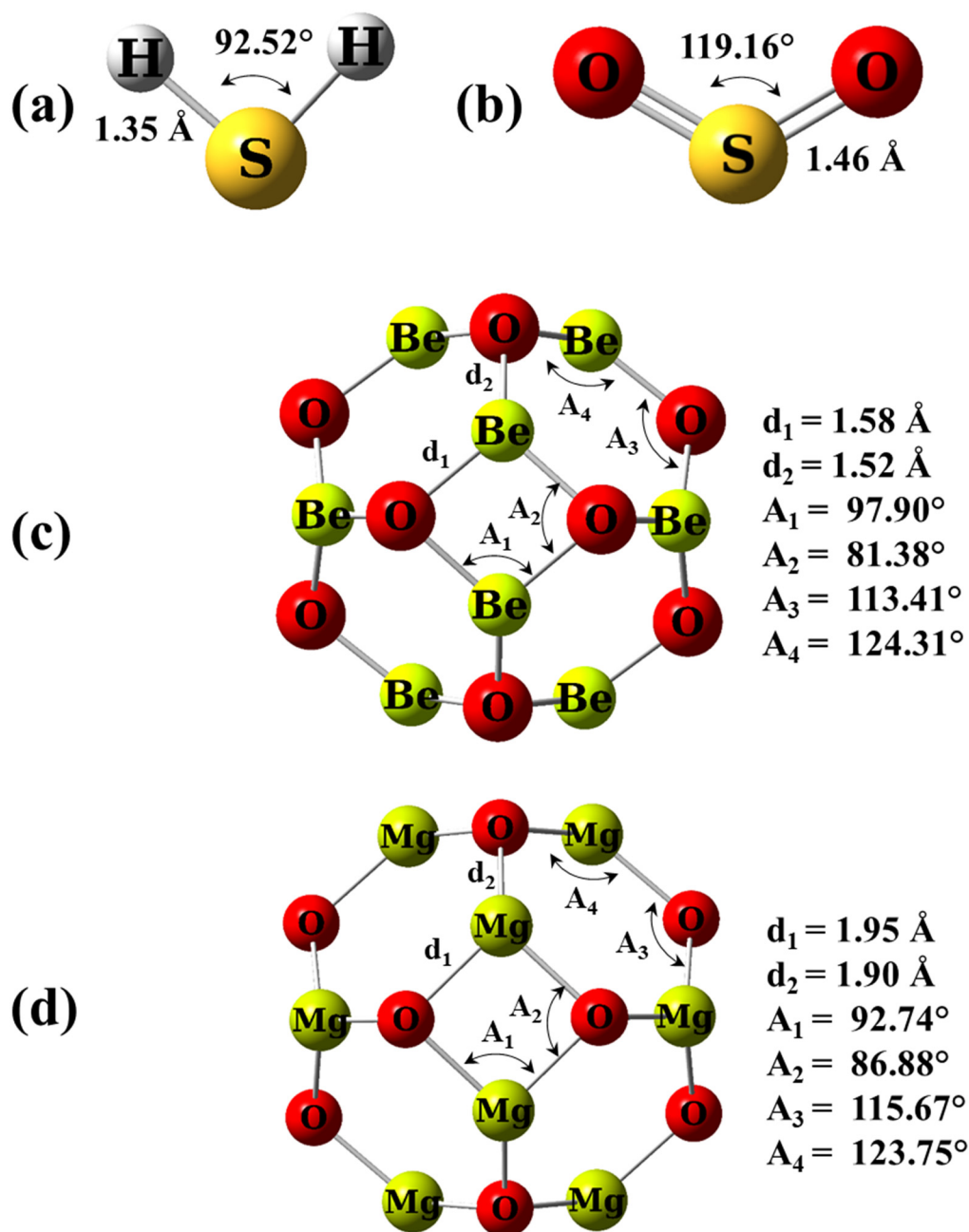


Figure 1. The optimized structures for (a) free H_2S gas, (b) free SO_2 gas, (c) $\text{Be}_{12}\text{O}_{12}$, and (d) $\text{Mg}_{12}\text{O}_{12}$ nano-cages.

It is clear that the S atom is surrounded by negative and positive electrostatic potentials for H_2S and SO_2 molecules, respectively. Furthermore, the MESP around the SO_2 molecule is extended in space more than that of the H_2S molecule.

Table 1. Electronic properties of Be₁₂O₁₂ and Mg₁₂O₁₂ nano-cages. HOMO and LUMO energy levels (eV), HOMO- LUMO gap (E_g, eV), ionization potential (IP, eV), NBO charges (Q, e), chemical potential (μ, eV), hardness (η, eV), electrophilicity (ω, eV), and dipole moment (D, Debye).

	Be ₁₂ O ₁₂		Mg ₁₂ O ₁₂	
	Present Study	Previous Studies	Present Study	Previous Studies
HOMO	−8.62	−8.62 [57]	−6.59	−6.58 [57], −6.57 [58], −6.60 [38], −6.58 [59], −6.74 [30,31], −6.53 [10], −1.78 [57], −1.71 [58], −1.80 [38], −1.72 [59]
LUMO	−0.79	−1.07 [57]	−1.75	4.87 [43], 4.83 [45], 4.79 [57], 4.86 [58,59], 4.78 [30,31]
E _g	7.83	8.29 [43], 7.41 [45], 7.55 [57]	4.84	
IP	10.27		7.98	
Q _M	1.19		1.44	
Q _O	−1.19		−1.44	
μ	−4.71		−4.17	−4.14 [58]
η	3.92		2.42	
ω	2.83		3.60	
D	0.00		0.01	0.01 [58], 0.00 [38], 0.07 [59]

M = Be and Mg.

For Be₁₂O₁₂ and Mg₁₂O₁₂ nano-cages, the O atoms and the metallic atoms are surrounded by negative and positive electrostatic potentials, respectively. In addition, the MESP of Mg₁₂O₁₂ is more extended around the nano-cage than that of the Be₁₂O₁₂ nano-cage. This is due to the higher charge polarization of Mg₁₂O₁₂. Therefore, it is expected that the S atoms of H₂S and SO₂ tend to be attracted to the metallic sites and oxygen sites of the nano-cages, respectively. Furthermore, the electric dipole moment (D) of Be₁₂O₁₂ and Mg₁₂O₁₂ nano-cages are 0.001 and 0.010 Debye, respectively. The low D values are owing to the uniform charge distribution on the nano-cages.

Molecular dynamic (MD) simulations examine the stability of the considered nano-cages at 300, 500, 700 K for a total time of 500 fs. Figure 3 depicts the fluctuation of the potential energy versus the time and the nano-cage geometric configuration at the end of the period.

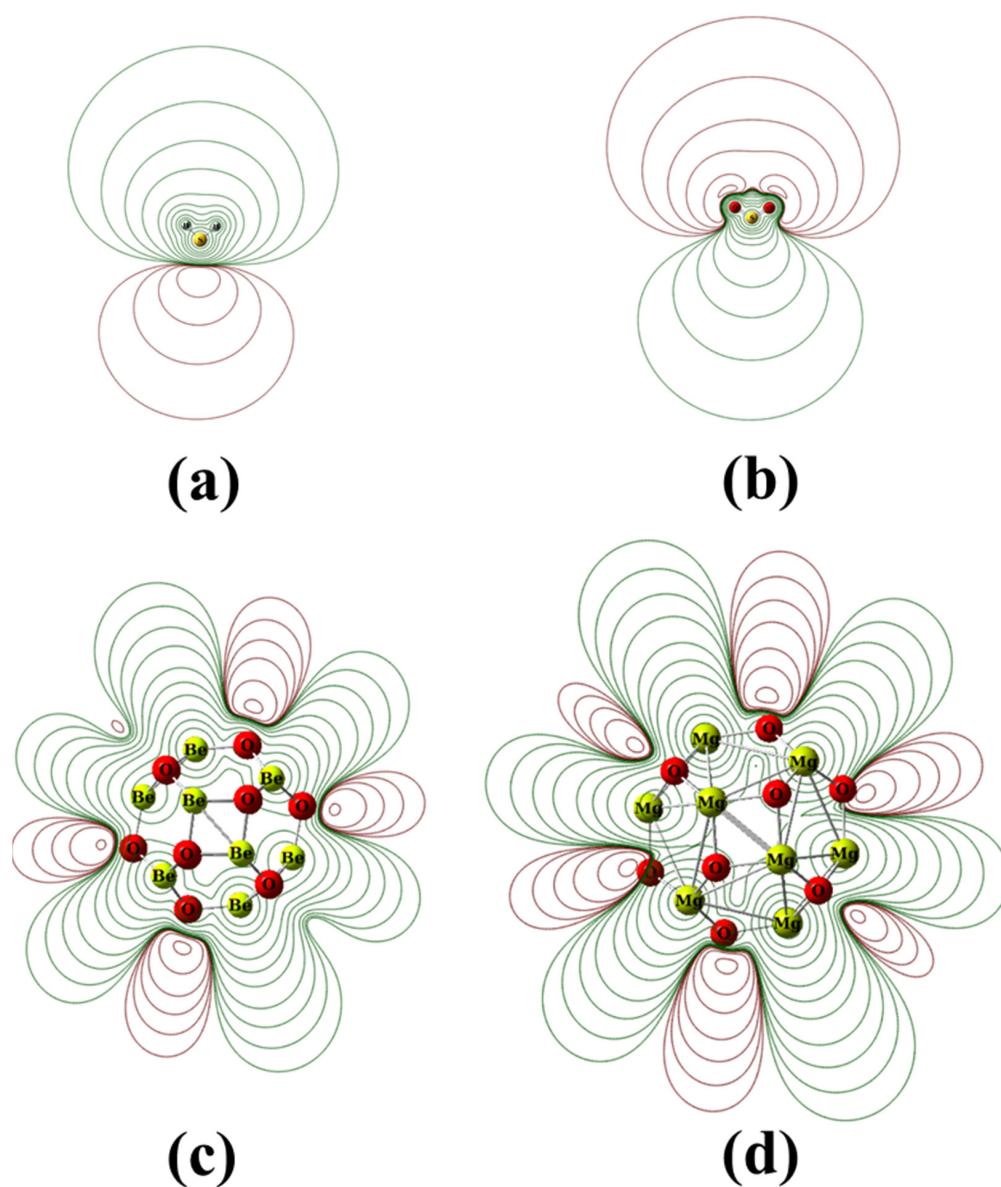


Figure 2. The molecular electrostatic potential contours (MESP) for (a) free H₂S gas, (b) free SO₂ gas, (c) Be₁₂O₁₂, and (d) Mg₁₂O₁₂ nano-cages at $\pm 0.001, \pm 0.002, \pm 0.004, \dots, \pm 0.8$ au iso-values. Red and green colors are assigned to negative and positive values, respectively.

It is obvious the potential energy trivially varies and no considerable distortion is observed for the nano-cages; this emphasizes the stability of Be₁₂O₁₂ and Mg₁₂O₁₂. In addition, the optimized geometries of discussed nano-cages were verified as true minima on the potential energy surfaces by the absence of imaginary frequencies [68–71].

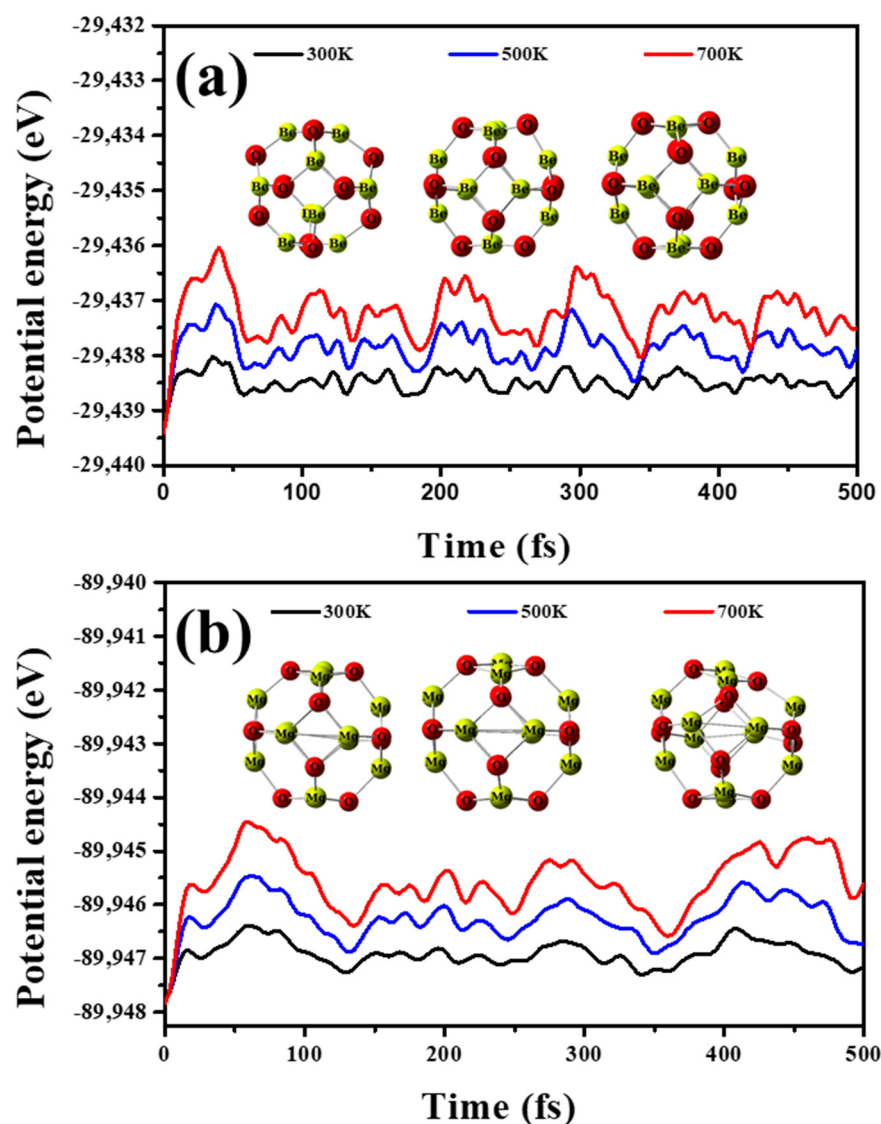


Figure 3. Potential energy fluctuations during MD simulation as well as the atomic configuration after 500 fs at 300, 500, and 700 K for (a) Be₁₂O₁₂, and (b) Mg₁₂O₁₂ nano-cages.

3.2. Adsorption of H₂S and SO₂ Gases

DFT as well DFT-D3 calculations were performed to investigate the adsorption characteristics of the adsorbed gases H₂S and SO₂ at the surfaces of Be₁₂O₁₂, as well Mg₁₂O₁₂, nano-cages. Four complexes are investigated—H₂S/Be₁₂O₁₂, H₂S/Mg₁₂O₁₂, SO₂/Be₁₂O₁₂, and SO₂/Mg₁₂O₁₂. There are several possibilities of the gas interaction with the nano-cage, therefore eight adsorption modes for each complex have been fully optimized without any restrictions. Tables S1 and S2 in the Supplementary Data show the examined adsorption modes for H₂S interaction with Be₁₂O₁₂ and Mg₁₂O₁₂, respectively. We found that the H₂S prefers to interact via its S atom toward the metallic atom Be or Mg of the nano-cage. Tables S3 and S4 in the Supplementary Data show the examined adsorption modes for SO₂ interaction with Be₁₂O₁₂ and Mg₁₂O₁₂, respectively. One can observe that SO₂ prefers to interact via its S and O atoms toward the O sites and the metallic atoms, respectively, of the nano-cages. The differences in total electronic energies (ΔE) for the examined orientations are shown in Figure 4.

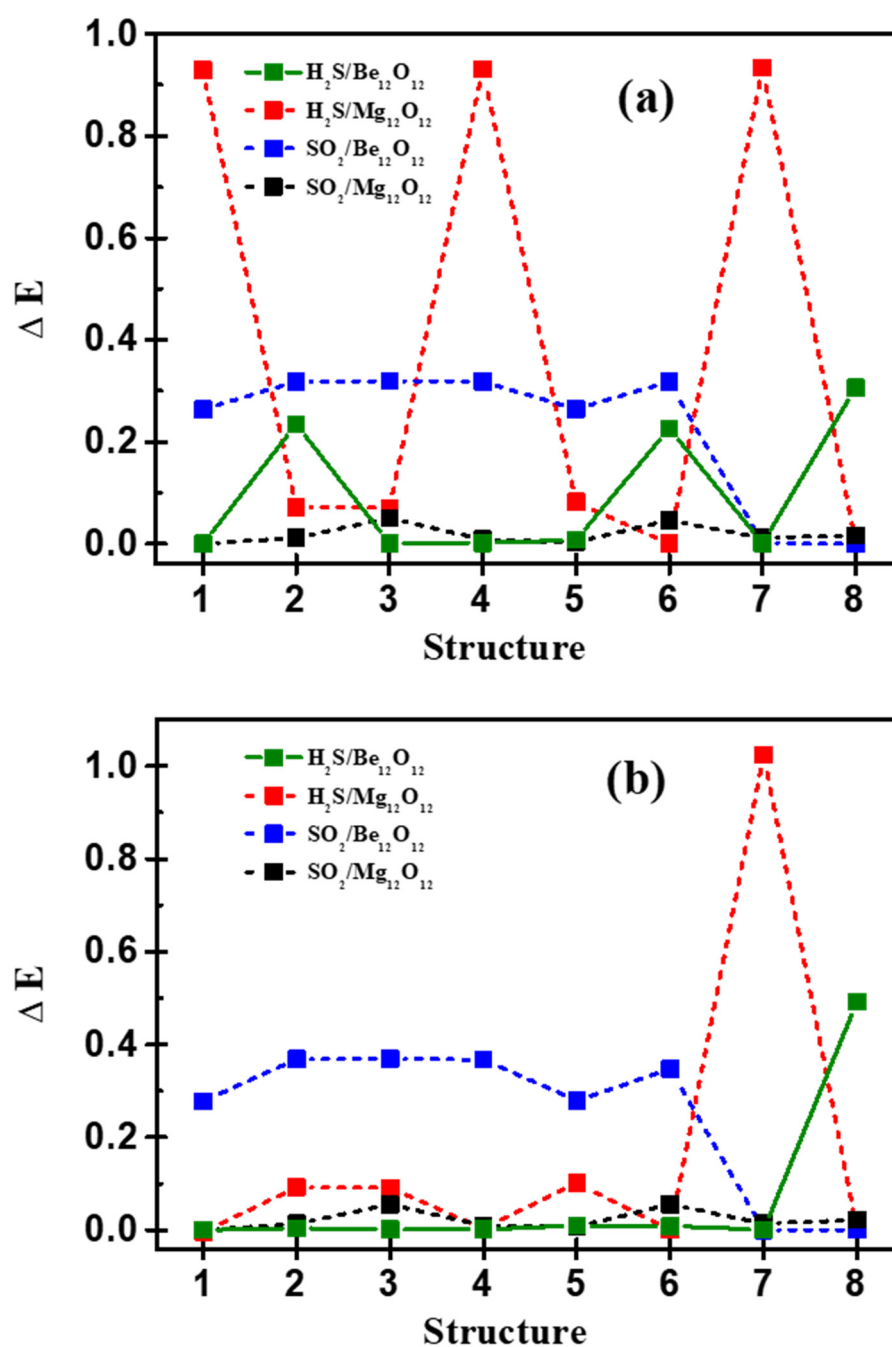


Figure 4. The differences in total electronic energies (ΔE) for the examined structures calculated at (a) DFT and (b) DFT-D3.

DFT and DFT-D3 calculations show that modes 1, 6, 8, and 1 for $\text{H}_2\text{S}/\text{Be}_{12}\text{O}_{12}$, $\text{H}_2\text{S}/\text{Mg}_{12}\text{O}_{12}$, $\text{SO}_2/\text{Be}_{12}\text{O}_{12}$, and $\text{SO}_2/\text{Mg}_{12}\text{O}_{12}$, respectively, are the most energetically stable adsorption modes. Figure 5 presents the most energetically stable adsorption modes that have more negative adsorption energy for each complex.

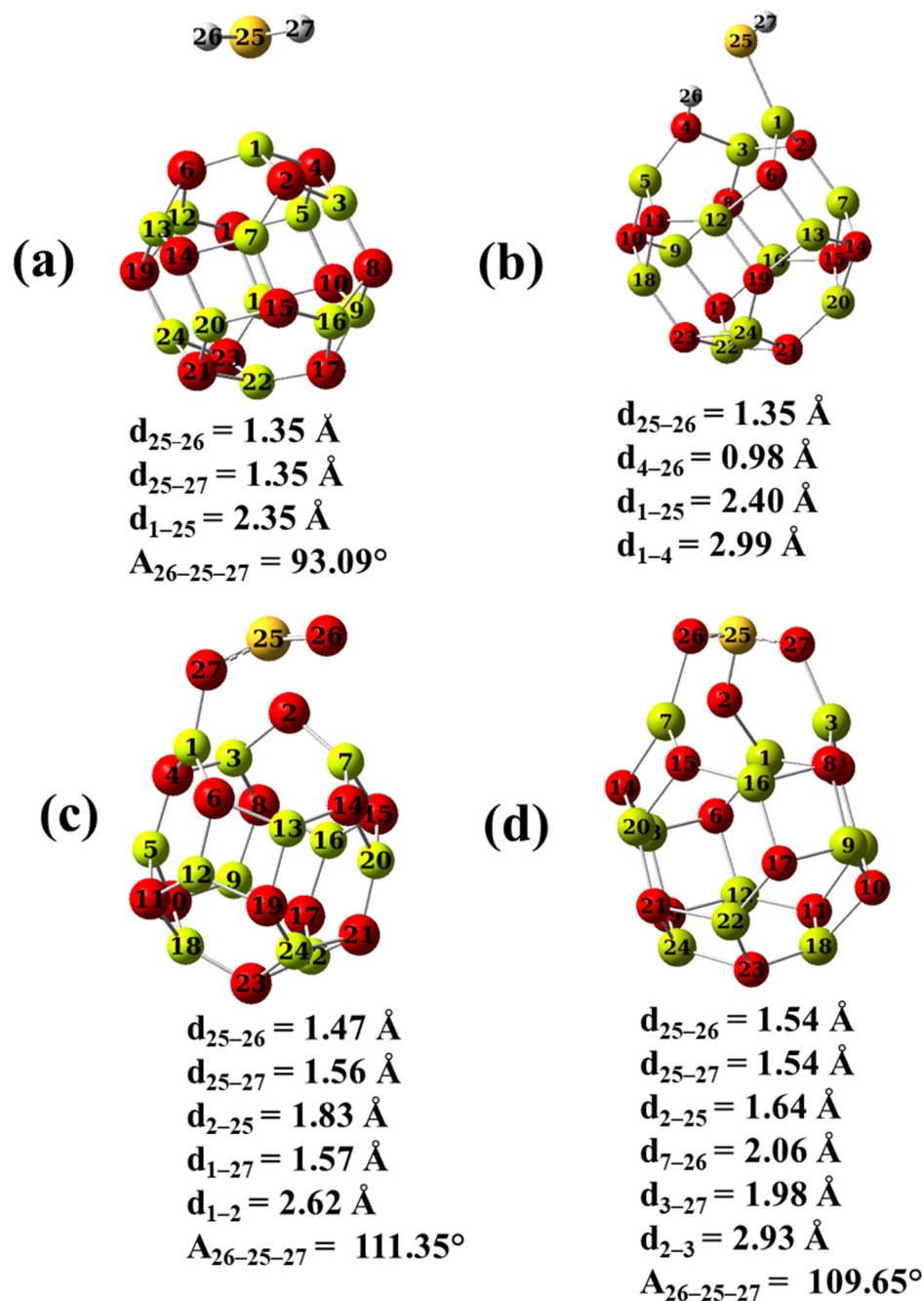


Figure 5. The optimal structures for (a) $\text{H}_2\text{S}/\text{Be}_{12}\text{O}_{12}$, (b) $\text{H}_2\text{S}/\text{Mg}_{12}\text{O}_{12}$, (c) $\text{SO}_2/\text{Be}_{12}\text{O}_{12}$, and (d) $\text{SO}_2/\text{Mg}_{12}\text{O}_{12}$ complexes.

Table 2 list the adsorption properties of H_2S and SO_2 . Notably, the DFT-D3 calculations give more negative adsorption energy values than DFT calculations.

Table 2. Adsorption properties of H₂S as well SO₂ on Be₁₂O₁₂ and Mg₁₂O₁₂ nano-cages. Adsorption energies (E_{ads}, eV), Basis set superposition error (BSSE, eV), corrected adsorption energy (E_{ads}^{corr}, eV), HOMO and LUMO energy levels (eV), HOMO- LUMO gap (E_g, eV), NBO charges (Q, e), and dipole moment (D, Debye).

	H ₂ S	H ₂ S/Be ₁₂ O ₁₂	H ₂ S/Mg ₁₂ O ₁₂
E _{ads}	-	-0.31 (-0.50)	-1.32 (-1.57)
BSSE	-	0.05 (0.05)	0.09 (0.10)
E _{ads} ^{corr}	-	-0.26 (-0.45)	-1.23 (-1.47)
HOMO	-7.31 (-7.31)	-8.20 (-8.22)	-5.93 (-5.95)
LUMO	0.26 (0.26)	-0.67 (-0.68)	-1.94 (-1.93)
E _g	7.56 (7.56)	7.53 (7.54)	3.99 (4.02)
Q _{H₂S}	0.00 (0.00)	0.23 (0.24)	-0.15 (-0.16)
D	1.33 (1.33)	3.27 (3.22)	5.50 (5.48)
	SO ₂	SO ₂ /Be ₁₂ O ₁₂	SO ₂ /Mg ₁₂ O ₁₂
E _{ads}	-	-0.83 (-1.07)	-2.33 (-2.52)
BSSE	-	0.38 (0.39)	0.41 (0.41)
E _{ads} ^{corr}	-	-0.45 (-0.68)	-1.93 (-2.11)
HOMO	-9.16 (-9.16)	-8.05 (-8.05)	-6.55 (-6.55)
LUMO	-3.73 (-3.73)	-1.47 (-1.49)	-1.84 (-1.83)
E _g	5.43 (5.43)	6.58 (6.57)	4.71 (4.72)
Q _{SO₂}	0.00 (0.00)	-0.13 (-0.13)	-0.34 (-0.34)
D	1.94 (1.94)	2.95 (2.83)	4.59 (4.58)

Values between brackets are calculated at B3LYP/6-311g(d,p) with dispersion correction (DFT-D3).

In contrast, the values for HOMO, LUMO, E_g, Q, and D have no considerable variations between DFT and DFT-D3 calculations. The E_{ads}^{corr} values show that the interaction of H₂S as well SO₂ at the surfaces of Be₁₂O₁₂ and Mg₁₂O₁₂ is a chemical interaction, where the E_{ads}^{corr} values are lower than -0.2 eV [67]. The released adsorption energy is in the following trend SO₂/Mg₁₂O₁₂ > H₂S/Mg₁₂O₁₂ > SO₂/Be₁₂O₁₂ > H₂S/Be₁₂O₁₂. One can notice that the ability of the Mg₁₂O₁₂ nano-cage to adsorb the considered gases is higher than that of the Be₁₂O₁₂ nano-cage. This is referred to as the higher ability of the Mg₁₂O₁₂ nano-cage to donate electrons than the Be₁₂O₁₂ nano-cage. Additionally, the ability of the SO₂ gas to be adsorbed on the Mg₁₂O₁₂ nano-cage, as well as the Be₁₂O₁₂ nano-cage, is higher than that of H₂S gas. Figure 5a shows that the H₂S/Be₁₂O₁₂ complex, the S atom of the H₂S molecule, is bonded to a Be site at a distance (d₁₋₂₅) of 2.35 Å, the S-H bond length is the same as that of the free H₂S molecule, and there is a negligible increase of the H-S-H angle. The H₂S molecule acquires a positive charge of 0.226 e, meaning that a charge transfer has occurred from the H₂S molecule to the Be₁₂O₁₂ nano-cage. Figure 5b illustrates the H₂S/Mg₁₂O₁₂ complex, while the H₂S molecule dissociates into two fragments HS and H. The HS fragment is bonded via its S atom to a Mg site at a distance (d₁₋₂₅) of 2.40 Å while the H fragment is attached to an O site at a distance (d₄₋₂₆) of 0.98 Å. Due to that, an obvious deformation has occurred in Mg₁₂O₁₂ where the Mg-O bond length (d₁₋₄) is elongated to 2.99 Å. The net acquired charge by the H₂S molecule is -0.146 e, which means the Mg₁₂O₁₂ donates a charge to the H₂S. Figure 5c demonstrates the SO₂/Be₁₂O₁₂ complex, while the S atom of the SO₂ molecule is bonded to an O site at a distance (d₂₋₂₅) of 1.83 Å, and an O atom of the SO₂ molecule is attached to a Be site at a distance (d₁₋₂₇) of 1.57 Å. While for the SO₂ molecule, the bond length (d₂₅₋₂₇) is stretched to 1.56 Å and the O-S-O angle is slightly widened to 111.35°. In addition, the Be-O bond length (d₁₋₂) is elongated to 2.62 Å. The SO₂ molecule gains a negative charge of 0.127 e, i.e., a charge transfer has occurred from the Be₁₂O₁₂ nano-cage to the SO₂ molecule. Furthermore, Figure 5d represents the SO₂/Mg₁₂O₁₂ complex; it seems that three bonds are formed between the SO₂ molecule and the Mg₁₂O₁₂ nano-cage. The two O atoms of the SO₂ molecule are bonded to two Mg sites at distances of (d₃₋₂₇) 1.98 Å and (d₇₋₂₆) 2.06 Å, while the S atom is attached to an O site at a distance (d₂₋₂₅) of 1.64 Å. In addition, the two S-O bonds of the SO₂ molecule are dilated to 1.54 Å while the O-S-O angle is diminished to 109.6° and the Mg-O bond length

(d_{2-3}) is elongated to 2.93 Å. Moreover, the SO_2 molecule accepts a negative charge of -0.339 e; therefore, a charge transfer has occurred from the $\text{Mg}_{12}\text{O}_{12}$ nano-cage to the SO_2 molecule. Additionally, the adsorption of H_2S leads to a decrease in the HOMO–LUMO gap (E_g) values of $\text{Be}_{12}\text{O}_{12}$ and $\text{Mg}_{12}\text{O}_{12}$ by 3.84% and 17.54%, respectively, whereas the adsorption of SO_2 leads to a decrease in E_g values by 15.97% and 2.60%, respectively. Therefore, one can say that the E_g of the $\text{Be}_{12}\text{O}_{12}$ nano-cage is more sensitive to the SO_2 than H_2S adsorption while the E_g of the $\text{Mg}_{12}\text{O}_{12}$ nano-cage reveals higher sensitivity to H_2S than SO_2 adsorption.

The electrical conductivity (σ) and recovery time (τ) are important aspects of sensing applications. σ depends on E_g according to the following equation [72–77]:

$$\Delta G = G_{\text{gas/nano-cage}} - (G_{\text{gas}} + G_{\text{nano-cage}}) \quad (10)$$

where A is a constant, k is Boltzmann's constant, and T is the temperature. Therefore, the increase of σ value of the $\text{Be}_{12}\text{O}_{12}$ nano-cage in the presence of SO_2 gas is higher than in the presence of H_2S gas, while the increase of σ value of the $\text{Mg}_{12}\text{O}_{12}$ nano-cage in the presence of H_2S gas is higher than in the presence of SO_2 gas. The τ is related to the E_{ads} as in Equation (11) [78,79]:

$$\tau = \nu_0^{-1} \exp\left(\frac{-E_{\text{ads}}}{KT}\right) \quad (11)$$

where ν_0 is the attempt frequency. In other words, as E_{ads} increases (more negative) the longer τ becomes. Therefore, in the obtained E_{ads} values, τ trends as follows: $\text{SO}_2/\text{Mg}_{12}\text{O}_{12} > \text{H}_2\text{S}/\text{Mg}_{12}\text{O}_{12} > \text{SO}_2/\text{Be}_{12}\text{O}_{12} > \text{H}_2\text{S}/\text{Be}_{12}\text{O}_{12}$. Thus, our results may be fruitful for sensing applications.

To illuminate the features of the interaction between the considered gases and the sorbent nano-cages, our results will be discussed related to the following: (i) NBO atomic charges as well charge density difference analysis ($\Delta\rho$), (ii) bond analysis, and (iii) PDOS analysis.

3.2.1. NBO and Charge Density Difference Analysis

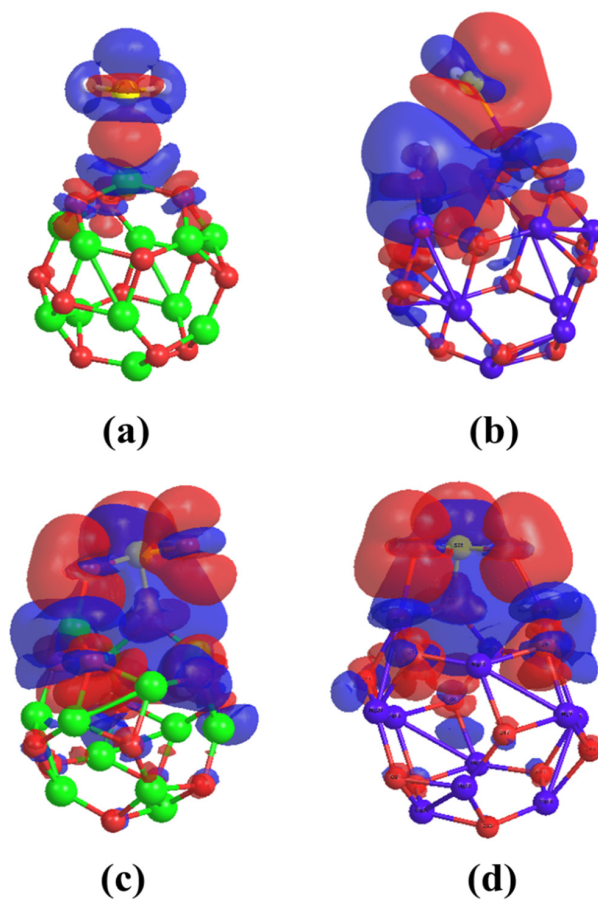
To shed light on the mechanism of H_2S and SO_2 interaction with the considered nano-cages, NBO analysis, as well as charge density difference ($\Delta\rho$) analysis, has been performed. Table 3 lists the atomic NBO charges, as well the electronic configuration of the atoms, for the free H_2S , $\text{Be}_{12}\text{O}_{12}$, $\text{Mg}_{12}\text{O}_{12}$, $\text{H}_2\text{S}/\text{Be}_{12}\text{O}_{12}$, and $\text{H}_2\text{S}/\text{Mg}_{12}\text{O}_{12}$. The numbering of atoms as shown in Figure 5 is used.

For the $\text{H}_2\text{S}/\text{Be}_{12}\text{O}_{12}$ structure, it is clear that due to the interaction, the 1s orbital of the H26 and H27 atoms loses charges of 0.03 and 0.02 e while the 3s and 3p orbitals of the S atom lose charges of 0.03 and 0.14 e, respectively. On the other hand, the 2s and 2p orbitals of the Be1 atom gain charges of 0.14 and 0.04 e while for the O2, O4, and O6 the 2s orbital loses a charge of 0.01e whereas the 2p orbital gains a charge of 0.01 e. This explains why a total charge of 0.226 e, as shown in Table 2, has been transferred from H_2S to the $\text{Be}_{12}\text{O}_{12}$ nano-cage and the major of the charge transfer has occurred from the S atom of H_2S to the Be1 atom of the $\text{Be}_{12}\text{O}_{12}$ nano-cage.

This means the major mechanism of the interaction is the charge transfer mechanism. In addition, a slight loss and gain of charges are observed simultaneously for the O2, O4, and O6; therefore, one can suggest another minor mechanism which is the donation–back donation mechanism. Figure 6a demonstrates $\Delta\rho$ for $\text{H}_2\text{S}/\text{Be}_{12}\text{O}_{12}$ complex.

Table 3. NBO charges (Q, e) and electronic configuration for free H₂S, Be₁₂O₁₂, Mg₁₂O₁₂, H₂S/Be₁₂O₁₂, and H₂S/Mg₁₂O₁₂.

Structure	Atom	Atomic Charge	Electronic Configuration				
			1s	2s	2p	3s	3p
H ₂ S	H	0.134	0.86	-	-	-	-
	S	-0.268	-	-	-	1.76	4.48
Be ₁₂ O ₁₂	Be	1.186	-	0.21	0.59	-	-
	O	-1.186	-	1.69	5.49	-	-
Mg ₁₂ O ₁₂	Mg	1.443	-	-	-	0.21	0.35
	O	-1.443	-	1.84	5.60	-	-
H ₂ S/Be ₁₂ O ₁₂	H26	0.160	0.83	-	-	-	-
	H27	0.159	0.84	-	-	-	-
	S	-0.093	-	-	-	1.73	4.34
	Be1	1.007	-	0.25	0.73	-	-
	O2	-1.191	-	1.68	5.50	-	-
	O4	-1.189	-	1.68	5.50	-	-
H ₂ S/Mg ₁₂ O ₁₂	O6	-1.190	-	1.68	5.50	-	-
	H26	0.509	0.49	-	-	-	-
	H27	0.130	0.86	-	-	-	-
	S	-0.785	-	-	-	1.81	4.97
	Mg1	1.305	-	-	-	0.27	0.41
	O2	-1.452	-	1.83	5.62	-	-
	O4	-1.251	-	1.77	5.47	-	-
	O6	-1.442	-	1.83	5.61	-	-

**Figure 6.** Charge density difference ($\Delta\rho$) for (a) H₂S/Be₁₂O₁₂, (b) H₂S/Mg₁₂O₁₂, (c) SO₂/Be₁₂O₁₂, and (d) SO₂/Mg₁₂O₁₂ complexes. Red color for negative $\Delta\rho$ and blue color for positive $\Delta\rho$.

The H and S atoms of the H₂S molecule are surrounded by positive $\Delta\rho$ values (blue color), which confirms the charge transfer from the H₂S molecule to the nano-cage. In addition, the positive (blue color) and negative (red color) $\Delta\rho$ values around each of the O₂, O₄, O₆, and S atoms confirm the donation–back donation mechanism. For H₂S/Mg₁₂O₁₂ structure, the interaction between H₂S and Mg₁₂O₁₂ leads to the following: the 1s orbital of the H₂₆ loses a charge of 0.37 e whereas the 2s and 2p of the O₄ atom lose a charge of 0.07 and 0.13 e, respectively. Furthermore, the H₂₇ atom has no change, the 3s and 3p orbitals of the S atom gain charges of 0.05 and 0.49 e, and the 3s and 3p of the Mg gain charges of 0.06 and 0.06 e, respectively. This confirms the dissociation of the H₂S molecule into H⁺ and SH[−]. Then, the H⁺ is attached to the O₄ atom, while the SH[−] is attached to the Mg₁ atom. Figure 6b shows $\Delta\rho$ for the H₂S/Mg₁₂O₁₂ complex. The H₂₆ is surrounded by positive $\Delta\rho$ values (blue color) while the S atom is surrounded by negative (red color) $\Delta\rho$ values which agree with the above discussion. Table 4 illustrates the atomic NBO charges, as well the electronic configuration of the atoms, for the free SO₂, Be₁₂O₁₂, Mg₁₂O₁₂, SO₂/Be₁₂O₁₂, and SO₂/Mg₁₂O₁₂.

Table 4. NBO charges (Q, e) and electronic configuration for free SO₂, Be₁₂O₁₂, Mg₁₂O₁₂, SO₂/Be₁₂O₁₂, and SO₂/Mg₁₂O₁₂.

Structure	Atom	Atomic Charge	Electronic Configuration			
			2s	2p	3s	3p
SO ₂	O	−0.747	1.84	4.89	-	-
	S	1.495	-	-	1.62	2.68
Be ₁₂ O ₁₂	Be	1.186	0.21	0.59	-	-
	O	−1.186	1.69	5.49	-	-
Mg ₁₂ O ₁₂	Mg	1.443	-	-	0.21	0.35
	O	−1.443	1.84	5.60	-	-
SO ₂ /Be ₁₂ O ₁₂	O ₂₆	−0.852	1.84	5.00	-	-
	O ₂₇	−0.980	1.76	5.21	-	-
	S	1.705	-	-	1.55	2.58
	Be ₁	1.210	0.22	0.55	-	-
	O ₂	−1.109	1.75	5.36	-	-
	O ₄	−1.214	1.69	5.52	-	-
	O ₆	−1.197	1.69	5.50	-	-
	O ₂₆	−1.003	1.82	5.17	-	-
	O ₂₇	−1.049	1.81	5.23	-	-
	S	1.713	-	-	1.51	2.62
SO ₂ /Mg ₁₂ O ₁₂	Mg ₁	1.477	-	-	0.20	0.32
	Mg ₃	1.468	-	-	0.20	0.32
	Mg ₇	1.417	-	-	0.21	0.36
	O ₂	−1.148	1.82	5.32	-	-
	O ₄	−1.463	1.84	5.62	-	-
	O ₈	−1.454	1.84	5.61	-	-

For SO₂/Be₁₂O₁₂ structure, one can observe, that the 2s of the O₂₇ and the 3s and 3p of the S atom lose charges of 0.08, 0.07, and 0.10 e, respectively, while the 2p of the O₂₆ and O₂₇ atoms gain charges of 0.11 and 0.32 e, respectively. Therefore, the positive charge of the S atom and the negative charge of the O₂₇ atom increase; consequently, they are attached to the O₂ negative and Mg₁ positive sites of the nano-cage, respectively. Moreover, for the Be₁ atom, the 2s gains a charge of 0.01 e while the 2p loses a charge of 0.04 e, whereas for the O₂ atom, the 2s gains a charge of 0.06 e while the 2p orbital loses a charge of 0.13 e. Therefore, one can say that there is a charge transfer from the Be₁₂O₁₂ nano-cage to the SO₂ molecule greater than the charge transferred from the SO₂ molecule to the Be₁₂O₁₂ nano-cage. This explains why SO₂ has a total charge of −0.127 e, as shown in Table 2. $\Delta\rho$ for the SO₂/Be₁₂O₁₂ complex is demonstrated in Figure 6c. It is clear that both the adsorbed SO₂ molecule and the sorbent Be₁₂O₁₂ nano-cage are surrounded by positive and negative $\Delta\rho$ values (blue and red colors) which confirms the donation–back donation

mechanism for the interaction. For the $\text{SO}_2/\text{Mg}_{12}\text{O}_{12}$ structure, one can notice that the 2s of the O26 and O27 loses charges of 0.02 and 0.03 e while the 2p gains charges of 0.28 and 0.34 e, respectively. Moreover, the 3s and 3p of the S atom lose charges of 0.11 and 0.06 e, respectively. Therefore, the net atomic charges of the O atoms of the SO_2 become more negative while the S atom becomes more positive, consequently, the O26 and O27 are attracted to the Mg7 and Mg3 positive sites while the S atom is attracted to the O2 negative site of the $\text{Mg}_{12}\text{O}_{12}$ nano-cage, whereas for the $\text{Mg}_{12}\text{O}_{12}$, the 2s and 2p of the O2 atom lose charges of 0.02 and 0.28 e while the rest atoms of the nano-cage have little gains and loss of charges. $\Delta\rho$ for the $\text{SO}_2/\text{Mg}_{12}\text{O}_{12}$ complex is illustrated in Figure 6d. It is clear that the adsorbed SO_2 molecule is surrounded by negative $\Delta\rho$ values greater than the positive $\Delta\rho$ values, which confirm the donation–back donation mechanism for the interaction.

3.2.2. Bond Analysis

Bond order and overlap population are estimated for the free adsorbed gasses as well gas/nano-cage complexes. As the overlap value decreases, the interaction between the two atoms decreases and vice versa whereas the values close to zero mean no interaction while overlapping positive and negative values indicate the bonding and anti-bonding states, respectively [71,75,80]. Table 5 concerns the free H_2S molecule, $\text{H}_2\text{S}/\text{Be}_{12}\text{O}_{12}$, and $\text{H}_2\text{S}/\text{Mg}_{12}\text{O}_{12}$ complexes.

Table 5. Overlap population and bond order of H_2S , $\text{H}_2\text{S}/\text{Be}_{12}\text{O}_{12}$, and $\text{H}_2\text{S}/\text{Mg}_{12}\text{O}_{12}$.

Structure	H_2S		$\text{H}_2\text{S}/\text{Be}_{12}\text{O}_{12}$		$\text{H}_2\text{S}/\text{Mg}_{12}\text{O}_{12}$	
	Overlap Pop.	Bond Order	Overlap Pop.	Bond Order	Overlap Pop.	Bond Order
S–H26	0.304	0.979	0.316	0.974	0.042	0.097
S–H27	0.304	0.979	0.313	0.972	0.266	0.956
S–M1	-	-	0.074	0.279	0.273	0.717
O4–H26	-	-	0.000	0.002	0.289	0.835
M1–O4	-	-	0.206 (0.220) *	0.538 (0.602) *	0.035 (0.183) *	0.106 (0.520) *

* Values between brackets are for the bare nano-cage. M = Be and Mg.

For $\text{H}_2\text{S}/\text{Be}_{12}\text{O}_{12}$, the overlap population and bond order values of the S–H26 and S–H27 bonds are slightly changed with respect to the free H_2S molecule, while overlapping population and bond order values of 0.074 and 0.279, respectively, are observed for the S–Be1 bond. This indicates the formation of a weak bond between the H_2S molecule and the $\text{Be}_{12}\text{O}_{12}$ nano-cage. On the other hand, for $\text{H}_2\text{S}/\text{Mg}_{12}\text{O}_{12}$, the low overlap population and bond order values for the S–H26 bond indicate the dissociation of the H_2S molecule. In addition, high overlapping population and bond order values for S–Mg1 and O4–H26 indicate bond formation between the S atom and the Mg1 atom and between the H26 atom and the O4 atom. Furthermore, the overlapping population and the bond order values for the Mg1–O4 are decreased to 0.035 and 0.106 rather than 0.183 and 0.520 for the bare nano-cage, respectively, indicating a bond weakness has occurred. This reveals the strong interaction between the H_2S molecule and the $\text{Mg}_{12}\text{O}_{12}$ nano-cage. Table 6 is interested in the free SO_2 molecule, $\text{SO}_2/\text{Be}_{12}\text{O}_{12}$, and $\text{SO}_2/\text{Mg}_{12}\text{O}_{12}$ complexes.

For $\text{SO}_2/\text{Be}_{12}\text{O}_{12}$, the S–O27 and Be1–O2 bonds are weakened as indicated by the low values of the overlap population and bond order, while the high overlap population and bond order values for the Be1–O27 bond indicate bond formation. On the other hand, for $\text{SO}_2/\text{Mg}_{12}\text{O}_{12}$, the decrease in the S–O26, S–O27, and Mg3–O2 overlapping population and bond order values indicates the weakness of these bonds while the bond order of 0.892, 0.464, and 0.495 for the S–O2, Mg–O27, and Mg–O26, respectively, confirms the formation of these bonds. In other words, one bond is formed between the SO_2 and the nano-cage for the $\text{SO}_2/\text{Be}_{12}\text{O}_{12}$ complex, whereas three bonds are formed for the $\text{SO}_2/\text{Mg}_{12}\text{O}_{12}$ complex. This explains the higher adsorption energy for $\text{SO}_2/\text{Mg}_{12}\text{O}_{12}$ than $\text{SO}_2/\text{Be}_{12}\text{O}_{12}$.

Table 6. Overlap population and bond order of SO₂, SO₂/Be₁₂O₁₂, and SO₂/Mg₁₂O₁₂.

Structure	SO ₂		SO ₂ /Be ₁₂ O ₁₂		SO ₂ /Mg ₁₂ O ₁₂	
	Overlap Pop.	Bond Order	Overlap Pop.	Bond Order	Overlap Pop.	Bond Order
S-O26	0.242	1.773	0.302	1.706	0.203	1.290
S-O27	0.242	1.773	0.116	1.138	0.156	1.219
S-O2	-	-	-0.015	0.564	0.079	0.892
M1-O27	-	-	0.262	0.614	0.000	-0.010
M3-O27	-	-	0.022	0.022	0.192	0.464
M7-O26	-	-	0.057	0.118	0.207	0.495
M1-O2	-	-	-0.006 (0.220) *	0.028 (0.602) *	0.113 (0.183) *	0.267 (0.520) *
M3-O2	-	-	0.215 (0.220) *	0.452 (0.602) *	0.033 (0.183) *	0.103 (0.520) *

* Values between brackets are for the bare nano-cage. M = Be and Mg.

3.2.3. PDOS Analysis

Figure 7 illustrates the surfaces of the HOMO and LUMO as well as the PDOS for the free H₂S molecule, the bare Be₁₂O₁₂, and Mg₁₂O₁₂ nano-cages, as well the H₂S/Be₁₂O₁₂ and H₂S/Mg₁₂O₁₂ complexes.

Figure 7a shows three occupied states for the H₂S molecule at -12.36, -10.12, and -7.30 eV; the H atom states located at -12.36 and -10.12 eV; and the S atom states located at -12.36, -10.12, and -7.35 eV. The S atom states for free H₂S molecule are disappeared in the H₂S/Be₁₂O₁₂ complex, as shown in Figure 7c. Furthermore, new states for the S atom are observed in the H₂S/Be₁₂O₁₂ complex; these states overlap with the Be and O states, which emphasizes the interaction between the H₂S molecule with the nano-cage. For instance, the states of the S, Be, and O atoms of the complex are overlapped at -8.20 eV, which is the HOMO of the complex. The HOMO surface of the complex displays the contribution of the S, Be, and O atoms. Comparing Figure 7b,c, one can observe the adsorption of the H₂S molecule rises the HOMO and LUMO of Be₁₂O₁₂ by 0.43 and 0.13 eV, respectively; therefore, a decrease of 0.30 eV in the HOMO-LUMO gap has been recorded. For H₂S/Mg₁₂O₁₂ complex, Figure 7e, it is clear that there is an overlap between the H and O states at -12.92 eV, which is due to the interaction between H26 and O4 in the complex. Moreover, the occupied states of the S atom are located at -9.70, -6.51, and -5.93 eV, i.e., they are shifted up with respect to the free H₂S, which confirms the strong interaction between the H₂S and Mg₁₂O₁₂ nano-cage. In addition, comparing Figure 7d,e, one can see that HOMO rises by 1.02 eV while LUMO lowers by 0.19 eV. Thus, H₂S adsorption narrows the HOMO-LUMO gap by 0.85 eV. It is worth noticing that only the states of S and O atoms appear in the HOMO states, and this agrees with the obtained HOMO surface for the H₂S/Mg₁₂O₁₂ complex. Figure 8 demonstrates the surfaces of HOMO and LUMO, as well PDOS, for the free SO₂ molecule, bare Be₁₂O₁₂, and Mg₁₂O₁₂ nano-cages, as well SO₂/Be₁₂O₁₂ and SO₂/Mg₁₂O₁₂ complexes.

Comparing Figure 8a-c, it is clear that there are dramatic changes in the states due to the adsorption of the SO₂ molecule on the Be₁₂O₁₂ nano-cage, where the states of SO₂ overlap with the states of Be₁₂O₁₂. For example, one can observe the appearance of the S atom and the O atoms of the SO₂ and Be₁₂O₁₂ in the HOMO states of the SO₂/Be₁₂O₁₂ at -8.05 eV. This is confirmed by the HOMO surface for the SO₂/Be₁₂O₁₂ complex. Based on the interaction, the HOMO of the nano-cage rises by 0.57 eV and the LUMO lowers by 0.68 eV, in turn, narrowing the HOMO-LUMO gap by 1.25 eV. Comparing Figure 8a,d,e, one can observe that adsorption of the SO₂ molecule on the Mg₁₂O₁₂ nano-cage leads to intense changes in the states of the SO₂ as well as the states of the Mg₁₂O₁₂, which confirms the occurrence of a strong interaction. Moreover, the HOMO of the nano-cage increases by 0.04 while the LUMO decreases by 0.08 eV; consequently, the HOMO-LUMO gap is slightly decreased by 0.12 eV.

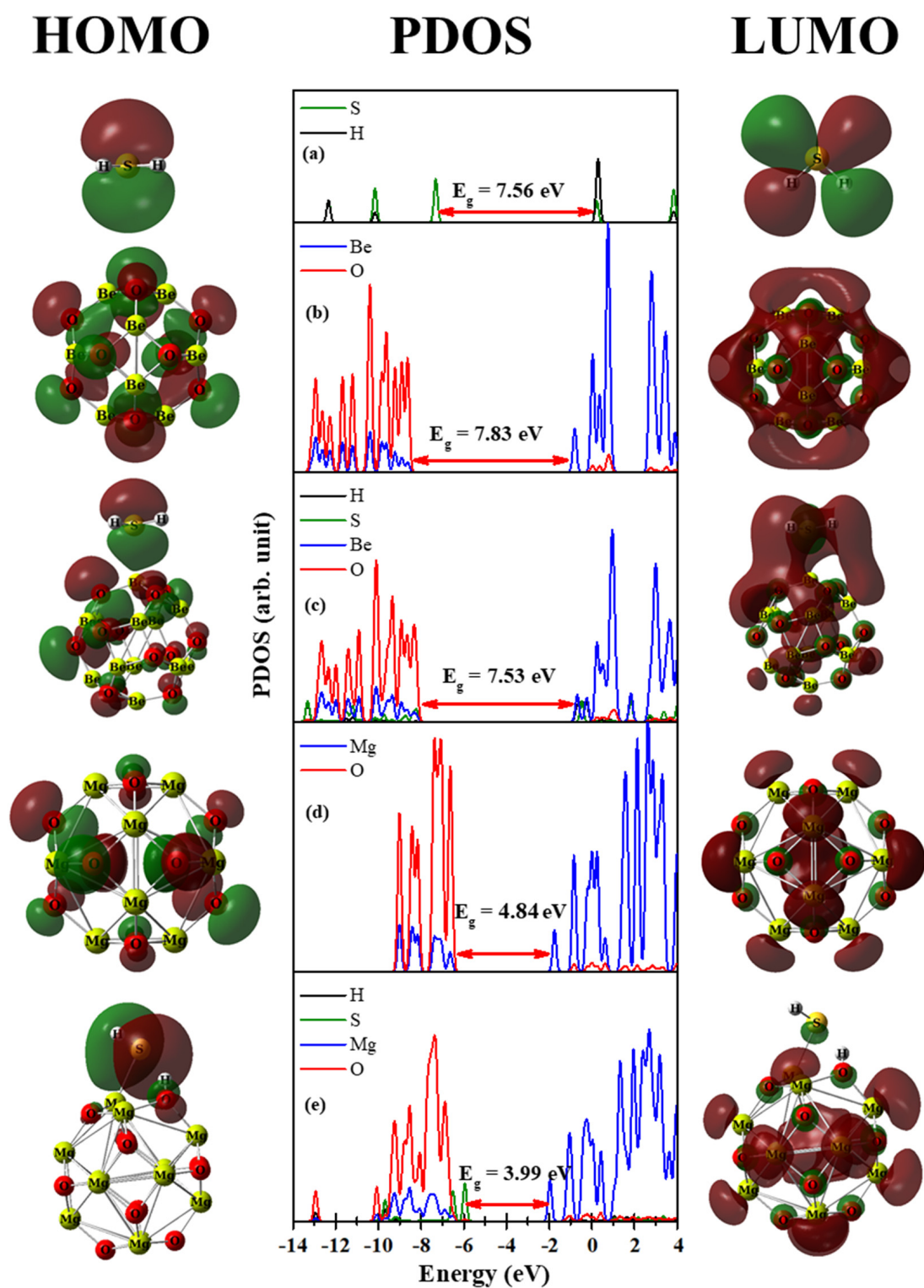


Figure 7. HOMO, PDOS, LUMO for (a) H_2S , (b) $\text{Be}_{12}\text{O}_{12}$, (c) $\text{H}_2\text{S}/\text{Be}_{12}\text{O}_{12}$, (d) $\text{Mg}_{12}\text{O}_{12}$, and (e) $\text{H}_2\text{S}/\text{Mg}_{12}\text{O}_{12}$ complexes.

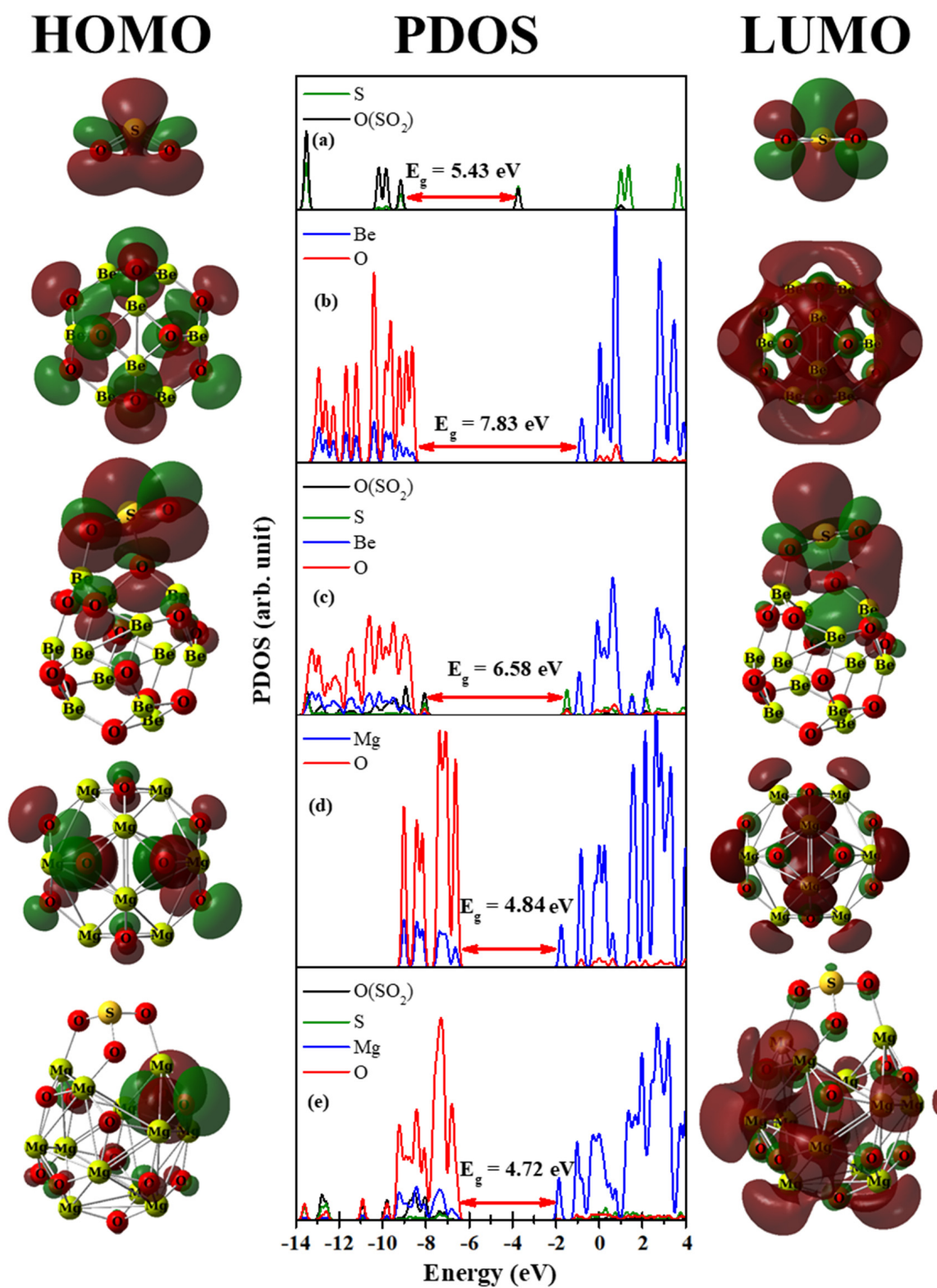


Figure 8. HOMO, PDOS, LUMO for (a) SO_2 , (b) $\text{Be}_{12}\text{O}_{12}$, (c) $\text{SO}_2/\text{Be}_{12}\text{O}_{12}$, (d) $\text{Mg}_{12}\text{O}_{12}$, and (e) $\text{SO}_2/\text{Mg}_{12}\text{O}_{12}$ complexes.

3.3. Molecular Dynamic Simulations

To examine the impact of the temperature on the adsorption process of the investigated gases, molecular dynamic (MD) simulations at 300, 500, and 700 K for a total time of 500 fs are performed for $\text{H}_2\text{S}/\text{Be}_{12}\text{O}_{12}$, $\text{H}_2\text{S}/\text{Mg}_{12}\text{O}_{12}$, $\text{SO}_2/\text{Be}_{12}\text{O}_{12}$, and $\text{SO}_2/\text{Mg}_{12}\text{O}_{12}$ complexes. MD simulations are carried out via the ADMP model. Figure 9a,b illustrates the potential energy fluctuations for $\text{H}_2\text{S}/\text{Be}_{12}\text{O}_{12}$ and $\text{H}_2\text{S}/\text{Mg}_{12}\text{O}_{12}$, respectively, as well as the atomic configuration after 500 fs at the inspected temperatures.

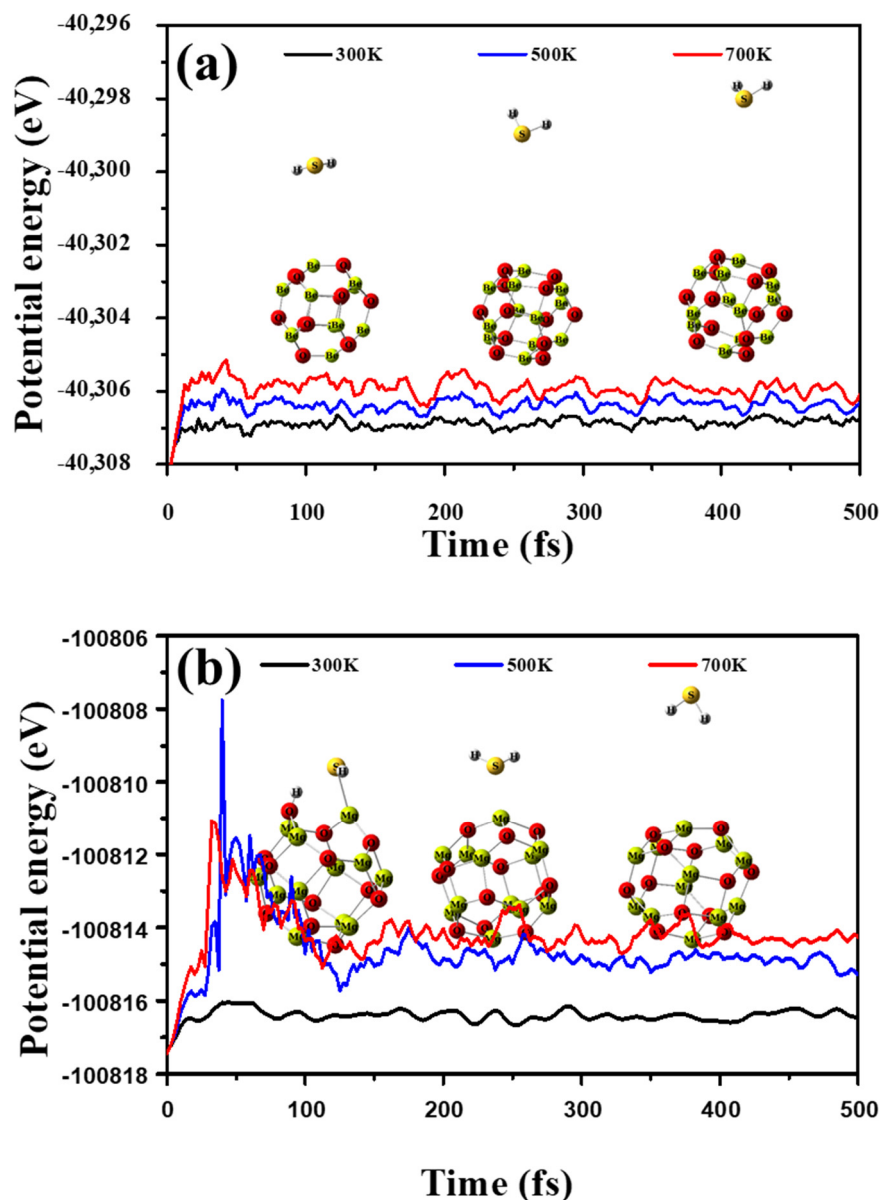


Figure 9. Potential energy fluctuations during MD simulation for (a) $\text{H}_2\text{S}/\text{Be}_{12}\text{O}_{12}$, and (b) $\text{H}_2\text{S}/\text{Mg}_{12}\text{O}_{12}$ and the atomic configuration after 500 fs at 300, 500, and 700 K.

For $\text{H}_2\text{S}/\text{Be}_{12}\text{O}_{12}$, Figure 9a, although the fluctuation of the potential energy is small, the distance (d_{1-25}) between H_2S and $\text{Be}_{12}\text{O}_{12}$ nano-cage increased with time. As well as the temperature increases, the increment in the distance increases, where the d_{1-25} values at the end of the time increase to 3.32, 7.38, and 9.55 Å for temperatures 300, 500, and 700 K, respectively. Therefore, one suggests that the $\text{Be}_{12}\text{O}_{12}$ nano-cage cannot retain H_2S on its surface, especially at high temperatures. For $\text{H}_2\text{S}/\text{Mg}_{12}\text{O}_{12}$, Figure 9b, at the temperature of 300 K, the fluctuation of the potential energy is small, and the $\text{Mg}_{12}\text{O}_{12}$

nano-cage preserves the dissociated H_2S molecule on its surface with no significant changes in the geometrical structure of the complex, while at the temperatures of 500 and 700 K, a high fluctuation of the potential energy is observed until 120–130 fs, when the fluctuation decreases. In addition, the dissociation of the H_2S molecule is diminished. At the end of the time, at 500 K, the H_2S is retained on the $\text{Mg}_{12}\text{O}_{12}$ nano-cage at a distance of 2.65 Å while at 700 K the d_{1-25} increases to 6.79 Å. Furthermore, Figure 10a,b demonstrates the potential energy fluctuations for $\text{SO}_2/\text{Be}_{12}\text{O}_{12}$ and $\text{SO}_2/\text{Mg}_{12}\text{O}_{12}$, respectively, as well as the atomic configuration after 500 fs at the inspected temperatures.

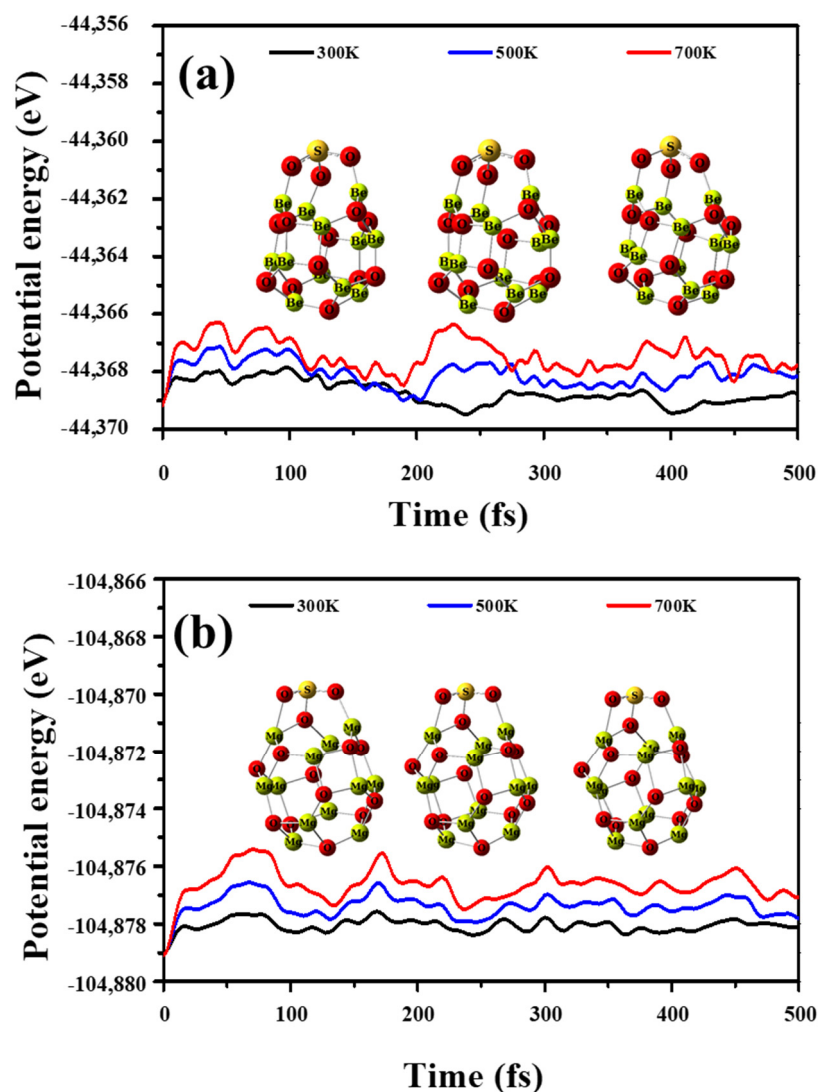


Figure 10. Potential energy fluctuations during MD simulation for (a) $\text{SO}_2/\text{Be}_{12}\text{O}_{12}$, and (b) $\text{SO}_2/\text{Mg}_{12}\text{O}_{12}$ and the atomic configuration after 500 fs at 300, 500, and 700 K.

It is clear that no significant fluctuation of the potential energy is observed. Moreover, at the end of the time, there is a trivial deformation in the geometrical structure of the $\text{SO}_2/\text{Be}_{12}\text{O}_{12}$ and $\text{SO}_2/\text{Mg}_{12}\text{O}_{12}$ complexes. Therefore, one proposes that $\text{Be}_{12}\text{O}_{12}$ and $\text{Mg}_{12}\text{O}_{12}$ nano-cages can retain the SO_2 molecule on their surface at temperatures up to 700 K.

3.4. Thermodynamic Properties

For gas adsorption, enthalpy difference (ΔH) and free energy difference (ΔG) are imperative thermodynamic parameters for determining the strength and the spontaneity of the reaction. Therefore, thermodynamic calculations for $\text{H}_2\text{S}/\text{Be}_{12}\text{O}_{12}$, $\text{H}_2\text{S}/\text{Mg}_{12}\text{O}_{12}$, $\text{SO}_2/\text{Be}_{12}\text{O}_{12}$, and $\text{SO}_2/\text{Mg}_{12}\text{O}_{12}$ complexes have been performed in the temperature range 300–700 K. Figure 11a signifies ΔH for the investigated complexes.

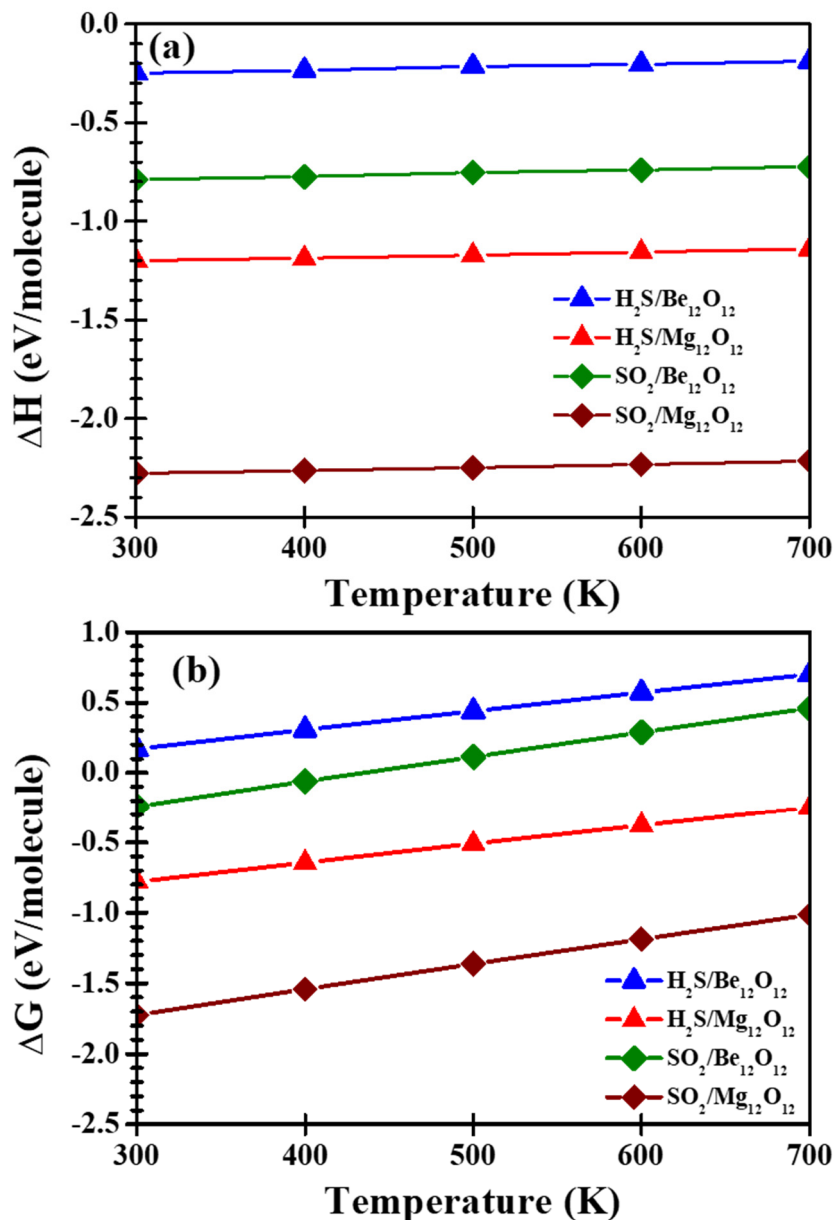


Figure 11. (a) ΔH and (b) ΔG for $\text{H}_2\text{S}/\text{Be}_{12}\text{O}_{12}$, $\text{H}_2\text{S}/\text{Mg}_{12}\text{O}_{12}$, $\text{SO}_2/\text{Be}_{12}\text{O}_{12}$, and $\text{SO}_2/\text{Mg}_{12}\text{O}_{12}$ complexes.

ΔH values for all considered complexes are negative, which specifies the reactions between H_2S as well SO_2 with $\text{Be}_{12}\text{O}_{12}$ and $\text{Mg}_{12}\text{O}_{12}$ nano-cages are exothermic. Furthermore, as the temperature increases, the negative ΔH values decrease, which indicates the reactions are stronger at lower temperatures. In addition, for the same gas, ΔH values are more negative for the $\text{Mg}_{12}\text{O}_{12}$ nano-cage than the $\text{Be}_{12}\text{O}_{12}$ nano-cage, while for the same nano-cage, ΔH values are more negative for SO_2 gas than H_2S gas. This confirms the above discussion of the high ability of the $\text{Mg}_{12}\text{O}_{12}$ nano-cage to absorb the investigated gases and the high ability of the SO_2 gas to attach to the considered nano-cages. Figure 11b shows

ΔG for the examined complexes. Spontaneous and non-spontaneous reactions are characterized by negative and positive ΔG values, respectively, while low negative ΔG values indicate the capability to reverse the reaction [46,66–68]. For the $\text{H}_2\text{S}/\text{Be}_{12}\text{O}_{12}$ complex in the temperature range, ΔG values are positive, which indicates a non-spontaneous reaction, while for the $\text{SO}_2/\text{Be}_{12}\text{O}_{12}$ complex, the reaction is spontaneous at low temperatures, and beyond $T = 400$ K, the reaction turns into a non-spontaneous reaction. Furthermore, for the $\text{H}_2\text{S}/\text{Mg}_{12}\text{O}_{12}$ and $\text{SO}_2/\text{Mg}_{12}\text{O}_{12}$ complexes in the temperature range, ΔG values are negative, which indicates a spontaneous reaction. In addition, the reaction is capable of being reversed in the $\text{H}_2\text{S}/\text{Mg}_{12}\text{O}_{12}$ complex easier than in the $\text{SO}_2/\text{Mg}_{12}\text{O}_{12}$ complex.

4. Conclusions

Structural and electronic properties of the considered $\text{Be}_{12}\text{O}_{12}$ and $\text{Mg}_{12}\text{O}_{12}$ nano-cages as well their stability are scrutinized. $\text{Mg}_{12}\text{O}_{12}$ exhibits lower E_g , IP, η , and higher ω values than those for $\text{Be}_{12}\text{O}_{12}$; therefore, $\text{Mg}_{12}\text{O}_{12}$ is more reactive than the $\text{Be}_{12}\text{O}_{12}$ nano-cage. Molecular dynamics calculations emphasize the stability of the investigated nano-cages. In addition, the interaction of H_2S and SO_2 gases at the surfaces of the inspected nano-cages have been studied, and the features of the interaction are examined in the point of the NBO atomic charges, charge density difference analysis ($\Delta\rho$), bond analysis, and PDOS. $E_{\text{ads}}^{\text{corr}}$ values show that the ability of the $\text{Mg}_{12}\text{O}_{12}$ nano-cage to adsorb the considered gases is higher than that of the $\text{Be}_{12}\text{O}_{12}$ nano-cage. Furthermore, the ability of SO_2 gas to be adsorbed is higher than that of H_2S gas. Furthermore, H_2S gas dissociates at the $\text{Mg}_{12}\text{O}_{12}$ surface. In addition, adsorption of H_2S leads to a decrease in the HOMO–LUMO gap (E_g) values of $\text{Be}_{12}\text{O}_{12}$ and $\text{Mg}_{12}\text{O}_{12}$ by 3.84% and 17.54%, respectively, whereas the adsorption of SO_2 leads to a decrease in E_g values by 15.97% and 2.60%, respectively. At high temperatures, MD calculations declare that the $\text{Be}_{12}\text{O}_{12}$ and $\text{Mg}_{12}\text{O}_{12}$ nano-cages do not retain the H_2S on their surfaces, while SO_2 is retained at low and high temperatures. Moreover, the thermodynamic calculations show that the reactions between H_2S and SO_2 with $\text{Be}_{12}\text{O}_{12}$ and $\text{Mg}_{12}\text{O}_{12}$ nano-cages are exothermic. Furthermore, at the temperature range of 300–700 K, the H_2S reaction with $\text{Mg}_{12}\text{O}_{12}$ and $\text{Be}_{12}\text{O}_{12}$ is spontaneous and non-spontaneous, respectively, while the SO_2 reaction with $\text{Mg}_{12}\text{O}_{12}$ is spontaneous, whereas the SO_2 reaction with $\text{Be}_{12}\text{O}_{12}$ is spontaneous at temperatures up to 400 K. In addition, the reaction is capable to be reversed in the $\text{H}_2\text{S}/\text{Mg}_{12}\text{O}_{12}$ complex easier than in the $\text{SO}_2/\text{Mg}_{12}\text{O}_{12}$ complex.

Supplementary Materials: The following supporting information can be downloaded at: <https://www.mdpi.com/article/10.3390/nano12101757/s1>, Table S1. The examined orientations for H_2S interaction with $\text{Be}_{12}\text{O}_{12}$, Table S2. The examined orientations for H_2S interaction with $\text{Mg}_{12}\text{O}_{12}$, Table S3. The examined orientations for SO_2 interaction with $\text{Be}_{12}\text{O}_{12}$, Table S4. The examined orientations for SO_2 interaction with $\text{Mg}_{12}\text{O}_{12}$.

Author Contributions: Conceptualization, K.M.E. and H.Y.A.; methodology, H.M.B., K.M.E. and H.Y.A.; software, H.Y.A.; formal analysis, H.M.B., K.M.E., S.B. and H.Y.A.; investigation, H.M.B., K.M.E., S.B. and H.Y.A.; resources, H.M.B. and H.Y.A.; data curation, H.M.B., K.M.E. and H.Y.A.; writing—original draft preparation, H.M.B., K.M.E., S.B. and H.Y.A.; writing—review and editing, H.M.B., K.M.E., S.B. and H.Y.A.; visualization, H.M.B., K.M.E., S.B. and H.Y.A.; supervision, K.M.E. and H.Y.A.; project administration, H.M.B.; funding acquisition, H.M.B. and H.Y.A. All authors have read and agreed to the published version of the manuscript.

Funding: This research was funded by Deanship of Scientific Research at Najran University grant number NU/-/SERC/10/569.

Data Availability Statement: Not applicable.

Acknowledgments: The authors are thankful to the Deanship of Scientific Research at Najran University for funding this work under the General Research Funding program grant code (NU/-/SERC/10/569).

Conflicts of Interest: The authors declare no conflict of interest.

References

1. Greenwood, N.N.; Earnshaw, A. *Chemistry of the Elements*, 2nd ed.; Butterworth Heinemann: Oxford, UK, 1998; ISBN 0-7506-3365-4.
2. Villalba, G.; Ayres, R.U. Schroder, Accounting for fluorine: Production, use, and loss. *J. Ind. Ecol.* **2008**, *11*, 85–101. [[CrossRef](#)]
3. Zhang, X.X.; Gui, Y.G.; Dong, X.C. Preparation and application of TiO₂ nanotube array gas sensor for SF₆-insulated equipment detection: A review. *Nanoscale Res. Lett.* **2016**, *11*, 302. [[CrossRef](#)] [[PubMed](#)]
4. Gui, Y.G.; Tang, C.; Zhou, Q.; Xu, L.N.; Zhao, Z.Y.; Zhang, X.X. The sensing mechanism of N-doped SWCNTs toward SF₆ decomposition products: A first-principle study. *Appl. Surf. Sci.* **2018**, *440*, 846–852. [[CrossRef](#)]
5. Ranea, V.A.; Quiña, P.L.D.; Yalet, N.M. General adsorption model for H₂S, H₂Se, H₂Te, NH₃, PH₃, AsH₃ and SbH₃ on the V₂O₅ (0 0 1) surface including the van der Waals interaction. *Chem. Phys. Lett.* **2019**, *720*, 58–63. [[CrossRef](#)]
6. Salih, E.; Ayes, A.I. DFT investigation of H₂S adsorption on graphenenanosheets andnanoribbons: Comparative study. *Superlattices Microstruct.* **2020**, *146*, 106650. [[CrossRef](#)]
7. Ganji, M.D.; Danesh, N. Adsorption of H₂S molecules by cucurbituril: An ab initio vdW-DF study. *RSC Adv.* **2013**, *3*, 22031–22038. [[CrossRef](#)]
8. Faye, O.; Eduok, U.; Szpunar, J.; Samoura, A.; Beye, A. H₂S adsorption and dissociation on NH-decorated graphene: A first principles study. *Surf. Sci.* **2018**, *668*, 100–106. [[CrossRef](#)]
9. Stern, A.C.; Boubel, R.W.; Turner, D.B.; Fox, D.L. *Fundamentals of Air Pollution*, 2nd ed.; Academic Press: Warsaw, Poland, 1997.
10. Eid, K.; Ammar, H. Adsorption of SO₂ on Li atoms deposited on MgO (1 0 0) surface: DFT calculations. *Appl. Surf. Sci.* **2011**, *257*, 6049–6058. [[CrossRef](#)]
11. Li, L.; Moore, P. Putative biological roles of hydrogen sulfide in health and disease: A breath of not so fresh air? *Trends Pharmacol. Sci.* **2008**, *29*, 84–90. [[CrossRef](#)] [[PubMed](#)]
12. Ayes, A.I. H₂S and SO₂ adsorption on Cu doped MoSe₂: DFT investigation. *Phys. Lett. A* **2021**, *422*, 127798. [[CrossRef](#)]
13. Linn, W.S.; Avol, E.L.; Peng, R.-C.; Shamoo, D.A.; Hackney, J.D. Hackney, Replicated dose-response study of sulfur dioxide effects in normal, atopic, and asthmatic volunteers. *Am. Rev. Respir. Dis.* **1987**, *136*, 1127–1135. [[CrossRef](#)] [[PubMed](#)]
14. Noei, M. Different electronic sensitivity of BN and AlN nanoclusters to SO₂ gas: DFT studies. *Vacuum* **2016**, *135*, 44–49. [[CrossRef](#)]
15. Salih, E.; Ayes, A.I. CO, CO₂, and SO₂ detection based on functionalized graphene nanoribbons: First principles study. *Phys. E Low-Dimens. Syst. Nanostruct.* **2020**, *123*, 114220. [[CrossRef](#)]
16. Salimifard, M.; Rad, A.S.; Mahanpoor, K. Mahanpoor, Surface interaction of H₂S, SO₂, and SO₃ on fullerene-like gallium nitride (GaN) nanostructure semiconductor. *Solid State Commun.* **2017**, *265*, 6–11. [[CrossRef](#)]
17. Sun, S.; Zhang, D.; Li, C.; Wang, Y. DFT study on the adsorption and dissociation of H₂S on CuO(111) surface. *RSC Adv.* **2015**, *5*, 21806–21811. [[CrossRef](#)]
18. Zhang, H.; Cen, W.; Liu, J.; Guo, J.; Yin, H.; Ning, P. Adsorption and oxidation of SO₂ by graphene oxides: A van der Waals density functional theory study. *Appl. Surf. Sci.* **2015**, *324*, 61–67. [[CrossRef](#)]
19. Barelli, L.; Bidini, G.; de Arespachaga, N.; Pérez, L.; Sisani, E. Biogas use in high temperature fuel cells: Enhancement of KOH-KI activated carbon performance toward H₂S removal. *Int. J. Hydrogen Energy* **2017**, *42*, 10341–10353. [[CrossRef](#)]
20. Shi, L.; Yang, K.; Zhao, Q.; Wang, H.; Cui, Q. Characterization and mechanisms of H₂S and SO₂ adsorption by activated carbon, *Energy Fuels. Energy Fuels* **2015**, *29*, 6678–6685. [[CrossRef](#)]
21. Nguyen-Thanh, D.; Bandosz, T.J. Effect of transition-metal cations on the adsorption of H₂S in modified pillared clays. *J. Phys. Chem. B* **2003**, *107*, 5812–5817. [[CrossRef](#)]
22. Ozekmekci, M.; Salkic, G.; Fellah, M.F. Use of zeolites for the removal of H₂S: A mini-review. *Fuel Process. Technol.* **2015**, *139*, 49–60. [[CrossRef](#)]
23. Albargi, H.; Ammar, H.Y.; Badran, H.M.; Algadi, H.; Umar, A. p-CuO/n-ZnO Heterojunction Structure for the Selective Detection of Hydrogen Sulphide and Sulphur Dioxide Gases: A Theoretical Approach. *Coatings* **2021**, *11*, 1200. [[CrossRef](#)]
24. Tang, Q.-L.; Duan, X.-X.; Zhang, T.-T.; Fan, X.; Zhang, X. Comparative theoretical study of the chemistry of hydrogen sulfide on Cu (100) and Au (100): Implications for sulfur tolerance of water gas shift nanocatalysts. *J. Phys. Chem. C* **2016**, *120*, 25351–25360. [[CrossRef](#)]
25. Chen, S.; Sun, S.; Lian, B.; Ma, Y.; Yan, Y.; Hu, S. The adsorption and dissociation of H₂S on Cu (100) surface: A DFT study. *Surf. Sci.* **2014**, *620*, 51–58. [[CrossRef](#)]
26. Chen, H.; Pang, J.; Zhang, J.; Wei, G.; Wei, S.; Yan, J.; Jin, S. Exploring monolayer Janus MoSSe as potential gas sensor for Cl₂, H₂S and SO₂. *Comput. Theor. Chem.* **2022**, *1211*, 113665. [[CrossRef](#)]
27. Siddique, S.A.; Sajid, H.; Gilani, M.A.; Ahmed, E.; Arshad, M.; Mahmood, T. Sensing of SO₃, SO₂, H₂S, NO₂ and N₂O toxic gases through aza-macrocycle via DFT calculations. *Comput. Theor. Chem.* **2022**, *1209*, 113606. [[CrossRef](#)]
28. Cui, H.; Jiang, J.; Gao, C.; Dai, F.; An, J.; Wen, Z.; Liu, Y. DFT study of Cu-modified and Cu-embedded WSe₂ monolayers for cohesive adsorption of NO₂, SO₂, CO₂, and H₂S. *Appl. Surf. Sci.* **2022**, *583*, 152522. [[CrossRef](#)]
29. Korica, M.; Balić, I.; van Wyk, L.M.; van Heerden, D.P.; Nikolayenko, V.I.; Barbour, L.J.; Jednačak, T.; Đilović, I.; Balić, T. Inclusion of CO₂, NH₃, SO₂, Cl₂ and H₂S in porous N₄O₄-donor macrocyclic Schiff base. *Microporous Mesoporous Mater.* **2022**, *332*, 111708. [[CrossRef](#)]
30. Eid, K.; Ammar, H. A density functional study of NO₂ adsorption on perfect and defective MgO (100) and Li/MgO (100) surfaces. *Appl. Surf. Sci.* **2012**, *258*, 7689–7698. [[CrossRef](#)]

31. Ammar, H.; Eid, K. NO₂ interaction with Au atom adsorbed on perfect and defective MgO(100) surfaces: Density functional theory calculations. *J. Nanosci. Nanotechnol.* **2013**, *13*, 6660–6671. [[CrossRef](#)]
32. Eid, K.; Taha, H.; Kamel, M.; Ashour, A.; Halim, W.A. Abdel Halim, DFT calculations of the CO adsorption on Mn, Fe, Co, and Au deposited at MgO (1 0 0) and CdO (1 0 0). *Appl. Surf. Sci.* **2012**, *258*, 9876–9890. [[CrossRef](#)]
33. Eid, K.; Matlak, M.; Zieliński, J. Apex oxygen and effective pairing interaction among planar oxygen quasiparticles in copper oxide superconductors. *Phys. C Supercond.* **1994**, *220*, 61–66. [[CrossRef](#)]
34. Ammar, H.Y.; Badran, H.M.; Umar, A.; Fouad, H.; Alothman, O.Y. ZnO Nanocrystal-Based Chloroform Detection: Density Functional Theory (DFT) Study. *Coatings* **2019**, *9*, 769. [[CrossRef](#)]
35. Fadradi, M.A.; Movlaroooy, T. Ab initio study of adsorption of CO on BNNTs: For gas nanosensor applications. *Mater. Chem. Phys.* **2018**, *215*, 360–367. [[CrossRef](#)]
36. Sun, Y.F.; Liu, S.B.; Meng, F.L.; Liu, J.Y.; Jin, Z.; Kong, L.T.; Liu, J.H. Metal oxide nanostructures and their gas sensing properties: A review. *Sensors* **2012**, *12*, 2610–2631. [[CrossRef](#)] [[PubMed](#)]
37. Ammar, H.; Eid, K.; Badran, H. Interaction and detection of formaldehyde on pristine and doped boron nitride nano-cage: DFT calculations. *Mater. Today Commun.* **2020**, *25*, 101408. [[CrossRef](#)]
38. Shamlouei, H.R.; Nouri, A.; Mohammadi, A.; Tehrani, A.D. Influence of transition metal atoms doping on structural, electronic and nonlinear optical properties of Mg₁₂O₁₂ nanoclusters: A DFT study. *Phys. E* **2016**, *77*, 48–53. [[CrossRef](#)]
39. Ren, L.; Cheng, L.; Feng, Y.; Wang, X. Geometric and electronic structures of (BeO)_N (N = 2–12, 16, 20, and 24): Rings, double rings, and cages. *J. Chem. Phys.* **2012**, *137*, 014309. [[CrossRef](#)]
40. Ziemann, P.J.; Castleman, A.W., Jr. Stabilities and structures of gas phase MgO clusters. *J. Chem. Phys.* **1991**, *94*, 718–728. [[CrossRef](#)]
41. Lenglet, M. Iono-covalent character of the metal oxygen bonds in oxides: A comparison of experimental and theoretical data. *Act. Passiv. Electron. Compon.* **2004**, *27*, 1–60. [[CrossRef](#)]
42. Hwang, D.Y.; Mebel, A.M. Theoretical study of the reaction of beryllium oxide with methane. *Chem. Phys. Lett.* **2001**, *348*, 303–310. [[CrossRef](#)]
43. Jouypazadeh, H.; Farrokhpour, H. DFT and TD-DFT study of the adsorption and detection of sulfur mustard chemical warfare agent by the C₂₄, C₁₂Si₁₂, Al₁₂N₁₂, Al₁₂P₁₂, Be₁₂O₁₂, B₁₂N₁₂ and Mg₁₂O₁₂ nanocages. *J. Mol. Struct.* **2018**, *1164*, 227–238. [[CrossRef](#)]
44. Rezaei-Sameti, M.; Abdoli, S. The capability of the pristine and (Sc, Ti) doped Be₁₂O₁₂ nanocluster to detect and adsorb of Mercaptopyridine molecule: A first principle study. *J. Mol. Struct.* **2019**, *1205*, 127593. [[CrossRef](#)]
45. Ahangari, M.G.; Mashhadzadeh, A.H. Dynamics study on hydrogen storage capacity of C₂₄, B₁₂N₁₂, Al₁₂N₁₂, Be₁₂O₁₂, Mg₁₂O₁₂, and Zn₁₂O₁₂ nano-cages. *Int. J. Hydrogen Energy* **2020**, *45*, 6745–6756. [[CrossRef](#)]
46. Ammar, H.; Eid, K.; Badran, H. TM-doped Mg₁₂O₁₂ nano-cages for hydrogen storage applications: Theoretical study. *Results Phys.* **2022**, *35*, 105349. [[CrossRef](#)]
47. Fallahi, P.; Jouypazadeh, H.; Farrokhpour, H. Theoretical studies on the potentials of some nanocages (Al₁₂N₁₂, Al₁₂P₁₂, B₁₂N₁₂, Be₁₂O₁₂, C₁₂Si₁₂, Mg₁₂O₁₂ and C₂₄) on the detection and adsorption of Tabun molecule: DFT and TD-DFT study. *J. Mol. Liq.* **2018**, *260*, 138–148. [[CrossRef](#)]
48. Kohn, W.; Sham, L.J. Self-consistent equations including exchange and correlation effects. *Phys. Rev. A* **1965**, *140*, A1133–A1138. [[CrossRef](#)]
49. Grimme, S.; Antony, J.; Ehrlich, S.; Krieg, H. A consistent and accurate ab initio parametrization of density functional dispersion correction (DFT-D) for the 94 elements H–Pu. *J. Chem. Phys.* **2010**, *132*, 154104–154119. [[CrossRef](#)]
50. Becke, A.D. Density-functional thermochemistry. III. The role of exact exchange. *J. Chem. Phys.* **1993**, *98*, 5648–5652. [[CrossRef](#)]
51. Lee, C.; Yang, W.; Parr, R.G. Development of the Colle-Salvetti correlation-energy formula into a functional of the electron density. *Phys. Rev. B* **1988**, *37*, 785–789. [[CrossRef](#)]
52. Miehlich, B.; Savin, A.; Stoll, H.; Preuss, H. Preuss, Results obtained with the correlation-energy density functionals of Becke and Lee, Yang and Parr. *Chem. Phys. Lett.* **1989**, *157*, 200–206. [[CrossRef](#)]
53. Pearson, R.G. Absolute electronegativity and hardness correlated with molecular orbital theory. *Proc. Natl. Acad. Sci. USA* **1986**, *83*, 8440–8441. [[CrossRef](#)] [[PubMed](#)]
54. Parr, R.G.; Szentpály, L.V.; Liu, S. Electrophilicity, index. *J. Am. Chem. Soc.* **1999**, *121*, 1922–1924. [[CrossRef](#)]
55. Boys, S.F.; Bernardi, F.D. The calculation of small molecular interactions by the differences of separate total energies. Some procedures with reduced errors. *Mol. Phys.* **1970**, *19*, 553–566. [[CrossRef](#)]
56. Guo, C.; Wang, C. A theoretical study on cage-like clusters (C₁₂-Ti₆ and C₁₂-Ti₆⁺²) for dihydrogen storage. *Int. J. Hydrogen Energy* **2019**, *44*, 10763–10769. [[CrossRef](#)]
57. Frisch, M.; Trucks, G.; Schlegel, H.; Scuseria, G.; Robb, M.; Cheeseman, J.; Scalmani, G.; Barone, V.; Mennucci, B.; Petersson, G. *Gaussian 09, Revision D.01*; Gaussian, Inc.: Wallingford, CT, USA, 2009.
58. O’Boyle, N.M.; Tenderholt, A.L.; Langner, K.M. Cclib: A library for package-independent computational chemistry algorithms. *J. Comput. Chem.* **2008**, *29*, 839–845. [[CrossRef](#)]
59. Glendening, E.D.; Reed, A.E.; Carpenter, J.E.; Weinhold, F. *NBO Version 3.1*; Gaussian, Inc.: Wallingford, CT, USA, 2003.

60. Sajid, H.; Siddique, S.A.; Ahmed, E.; Arshad, M.; Gilani, M.A.; Rauf, A.; Imran, M.; Mahmood, F. DFT outcome for comparative analysis of $\text{Be}_{12}\text{O}_{12}$, $\text{Mg}_{12}\text{O}_{12}$ and $\text{Ca}_{12}\text{O}_{12}$ nanocages toward sensing of N_2O , NO_2 , NO , H_2S , SO_2 and SO_3 gases. *Comput. Theor. Chem.* **2022**, *1211*, 113694. [[CrossRef](#)]
61. Shakerzdeh, E.; Tahmasebi, E.; Shamlouei, H.R. Shamlouei, The influence of alkali metals (Li, Na and K) interaction with $\text{Be}_{12}\text{O}_{12}$ and $\text{Mg}_{12}\text{O}_{12}$ nanoclusters on their structural, electronic and nonlinear optical properties: A theoretical study. *Synth. Met.* **2015**, *204*, 17–24. [[CrossRef](#)]
62. Kakemam, J.; Peyghan, A.A. Electronic, energetic, and structural properties of C- and Si-doped $\text{Mg}_{12}\text{O}_{12}$ nano-cages. *Comput. Mater. Sci.* **2013**, *79*, 352–355. [[CrossRef](#)]
63. El-Gharkawy, E.-S.R.H.; Ammar, H. Adsorption of CO on TM-Deposited $(\text{MgO})_{12}$ Nano-Cage (TM = Ni, Pd and Pt): A Study on Electronic Properties. *J. Nanoelectron. Optoelectron.* **2018**, *13*, 546–553. [[CrossRef](#)]
64. Ammar, H.; Badran, H.; Eid, K. TM-doped $\text{B}_{12}\text{N}_{12}$ nano-cage (TM = Mn, Fe) as a sensor for CO, NO, and NH_3 gases: A DFT and TD-DFT study. *Mater. Today Commun.* **2020**, *25*, 101681. [[CrossRef](#)]
65. Yang, M.; Zhang, Y.; Huang, S.; Liu, H.; Wang, P.; Tian, H. Theoretical investigation of CO adsorption on TM-doped $(\text{MgO})_{12}$ (TM = Ni, Pd, Pt) nanotubes. *Appl. Surf. Sci.* **2011**, *258*, 1429–1436. [[CrossRef](#)]
66. Abbasi, M.; Nemati-Kande, E.; Mohammadi, M.D. Doping of the first row transition metals onto $\text{B}_{12}\text{N}_{12}$ nanocage: A DFT study. *Comput. Theor. Chem.* **2018**, *1132*, 1–11. [[CrossRef](#)]
67. Ammar, H.; Eid, K.; Badran, H. The impact of an external electric field on methanol adsorption on $\text{XB}_{11}\text{N}_{12}$ (X = B, Co, Ni) nano-cages: A DFT and TD-DFT study. *J. Phys. Chem. Solids* **2021**, *153*, 110033. [[CrossRef](#)]
68. Alam, M.S.; Lee, D.U. Molecular structure, spectral (FT-IR, FT-Raman, Uv-Vis, and fluorescent) properties and quantum chemical analyses of azomethine derivative of 4-aminoantipyrine. *J. Mol. Struct.* **2020**, *1227*, 129512. [[CrossRef](#)]
69. Balan, C.; Pop, L.-C.; Baia, M. IR, Raman and SERS analysis of amikacin combined with DFT-based calculations, *Spectrochimica Acta Part A Mol. Biomol. Spectrosc.* **2019**, *214*, 79–85. [[CrossRef](#)] [[PubMed](#)]
70. Yüksel, B. Spectroscopic characterization (IR and NMR), structural investigation, DFT study, and Hirshfeld surface analysis of two zinc(II) 2-acetylthiophenyl-thiosemicarbazone complexes. *J. Mol. Struct.* **2020**, *1229*, 129617. [[CrossRef](#)]
71. Badran, H.; Eid, K.; Ammar, H. DFT and TD-DFT studies of halogens adsorption on cobalt-doped porphyrin: Effect of the external electric field. *Results Phys.* **2021**, *23*, 103964. [[CrossRef](#)]
72. Kittel, C. *Introduction to Solid State Physics*; John Wiley and Sons: Hoboken, NJ, USA, 2005; pp. 216–226.
73. Kasap, S.O. *Principles of Electronic Materials and Devices*; McGraw-Hill: Boston, MA, USA, 2006; pp. 378–405.
74. Ammar, H.; Badran, H. Effect of CO adsorption on properties of transition metal doped porphyrin: A DFT and TD-DFT study. *Heliyon* **2019**, *5*, e02545. [[CrossRef](#)]
75. Guo, J.; Guan, L.; Wang, S.; Zhao, Q.; Wang, Y.; Liu, B. Study of hydrogen adsorption on the Ti (0 0 0 1)-(1 × 1) surface by density functional theory. *Appl. Surf. Sci.* **2008**, *255*, 3164–3169. [[CrossRef](#)]
76. Jigang, W.; Ji, L.; Yong, D.; Yan, Z.; Lihui, M.; Asadi, H. Effect of platinum on the sensing performance of ZnO nanocluster to CO gas. *Solid State Commun.* **2020**, *316–317*, 113954. [[CrossRef](#)]
77. Sconza, A.; Torzo, G. An undergraduate laboratory experiment for measuring the energy gap in semiconductors. *Eur. J. Phys.* **1989**, *10*, 123–126. [[CrossRef](#)]
78. Demir, S.; Fellah, M.F. A DFT study on Pt doped (4,0) SWCNT: CO adsorption and sensing. *Appl. Surf. Sci.* **2019**, *504*, 144141. [[CrossRef](#)]
79. Cui, H.; Zhang, G.; Zhang, X.; Tang, J. Rh-doped MoSe_2 as a toxic gas scavenger: A first-principles study. *Nanoscale Adv.* **2018**, *1*, 772–780. [[CrossRef](#)]
80. Segall, M.D.; Shah, R.; Pickard, C.J.; Payne, M.C. Population analysis of plane-wave electronic structure calculations of bulk materials. *Phys. Rev. B* **1996**, *54*, 16317–16320. [[CrossRef](#)] [[PubMed](#)]